Equivalence of light-front and covariant field theory

Bakker, B.L.G.; Ligterink, N.E.

published in
Physical Review D
1995

document version
Publisher's PDF, also known as Version of record

Equivalence of light-front and covariant field theory

N.E. Ligterink and B.L.G. Bakker
Department of Physics and Astronomy, Vrije Universiteit, Amsterdam, The Netherlands
(Received 21 December 1994)

In this paper we discuss the relation between the standard covariant quantum field theory and light-front field theory. We define covariant theory by its Feynman diagrams, whereas light-front field theory is defined in terms of light-cone time-ordered diagrams. A general algorithm is proposed that produces the latter from any Feynman diagram. The procedure is illustrated in several cases. Technical problems that occur in the light-front formulation and have no counterpart in the covariant formulation are identified and solved. The problem of renormalization is not discussed in this paper.

PACS number(s): 11.15.Bt, 03.70.+k, 11.10.Ef

I. INTRODUCTION

Dirac's paper [1] on forms of relativistic dynamics opened up a whole field of investigation: the study of different ways of quantizing and the relationship between different forms of dynamics. Three forms were identified: the instant form, that corresponds to ordinary time ordered theories, the point form, that will be of no concern to us here, and the front form, where the dynamical variables refer to physical conditions on a plane advancing with the velocity of light. (Such surfaces are called null planes or light fronts.) The latter form has the advantage that it requires only three dynamical operators, "Hamiltonians," the other seven (kinematical) generators of the Poincaré group containing no interaction. The other advantage noted by Dirac was that there is no square root in the Hamiltonians, thus avoiding the degeneracy of the free field solutions. (Particles and antiparticles cannot have the same kinematical momenta.)

Dirac published his paper right in the middle of the period in the development of quantum electrodynamics when old-fashioned perturbation theory was replaced by the covariant formalisms of Feynman, Schwinger, and Tomonaga [2]. Only much later were his ideas taken up again.[1] Quantum electrodynamics held center stage for a long time, not only for its unparalleled phenomenological success, but also because it functioned as a role model for many new theories, notably the gauge theories of the weak and the strong interactions.

A new development occurred when the infinite-momentum frame, which had appeared in connection with current algebra (see, e.g., de Alfaro *et al.* [5]), was proposed by Weinberg [6] as a tool in the study of scalar theories, because it simplifies the vacuum structure in those theories. Not long after Weinberg's paper was published, it was suggested [7] that the use of a new set of variables, viz.,

$$x^+ = \frac{x^0 + x^3}{\sqrt{2}},\ x^- = \frac{x^0 - x^3}{\sqrt{2}},\ x^1,\ x^2, \tag{1}$$

would provide the advantages which are present in the use of the infinite-momentum frame. In such a description, x^+ plays the role of "time," i.e., the evolution parameter, and the connection to Dirac's front form of dynamics seems immediate. [We will use the terminology light-cone time (LCT) for this variable.] However, the connection between the rest frame and the infinite-momentum frame involves a limiting procedure of Lorentz transformations. Therefore, the equivalence of descriptions in those frames cannot be derived using arguments based on Lorentz invariance alone.

So the question concerning the relationship between different forms of dynamics remains difficult to answer. In particular, the connection between the manifestly covariant formulations and the front form is not yet fully clear. The main reason is that quantization using planes $x^+ = \tau$ as surfaces on which the initial conditions are specified, initial surfaces, is beset with difficulties that occur already at the classical level in scalar theories. It is a well established result from the theory of partial-differential equations [8] that the Cauchy problem with an initial surface that contains a lightlike direction is ill posed.

Attempts to formulate light-front field theory in close relationship with covariant field theory were made by, e.g., Chang *et al.* [9], Robertson and McCartor, and Brodsky and Langnau [10]. However, in these approaches one encounters some difficulties, e.g., the ill posedness of the Cauchy problem, discussed above, the occurrence of ill-defined space-time objects such as $\epsilon(x^- - y^-)\delta^2(x_\perp - y_\perp)$ in the operator $1/p^+$, and the closely related problem of noncovariantly normalized states [11].

This disturbing fact might hinder the development of a Hamiltonian formulation of front-form field theory, if it could not be circumvented. A possible way out was shown by Chang and Ma [7] and later by Kogut and Soper [12]: one may attack the problem at the level of Feynman diagrams. If one follows this line, one must show that the usual Feynman rules can be reformulated

[1] Leutwyler and Stern [3] extended Dirac's analysis to include two more forms of dynamics. A review on the present situation can be found in [4].

in terms of the new variables, Eq. (1), or their conjugate momenta

$$p^+ = \frac{p^0 + p^3}{\sqrt{2}}, \quad p^- = \frac{p^0 - p^3}{\sqrt{2}}, \quad p^1, \; p^2. \tag{2}$$

In this paper we use their approach. We avoid the problems of quantization and assume that covariant quantization is correct. Then we show that the perturbative expansion in covariant terms, Feynman diagrams, is equivalent to an expansion in light-cone time-ordered terms for theories describing spinless particles. We show in Sec. II how to derive light-cone time-ordered (LCT-ordered) diagrams from a given Feynman diagram by integrating over the LC energy p^-. The general algorithm is illustrated there by applying it to the box diagram. On the way to the proof of equivalence we encounter questions of regularization. For scalar theories they are not more difficult to answer than in the manifestly covariant formulation.

The true difficulty lies in theories containing spinning particles. In the case of spin-$\frac{1}{2}$ particles one encounters the following expression for the free propagator [12]:

$$\begin{aligned}\frac{i(\not{p} + m)}{p^2 - m^2 + i\epsilon} &= \frac{i(\not{p}_{\rm on} + m)}{p^2 - m^2 + i\epsilon} + \frac{i\gamma^+}{2p^+} \\ &= \sum_\alpha \frac{iu^{(\alpha)} \otimes \bar{u}^{(\alpha)}}{p^2 - m^2 + i\epsilon} + \frac{i\gamma^+}{2p^+},\end{aligned} \tag{3}$$

where $p_{\rm on}$ is the on-shell value of the four-momentum of the spin-$\frac{1}{2}$ particle with mass m, if its components p^+, p^1, and p^2 are given. The component $p^-_{\rm on}$ is computed from

$$p^2 = 2p^+p^- - p_\perp^2 = m^2 \tag{4}$$

and so

$$p^-_{\rm on} = \frac{p_\perp^2 + m^2}{2p^+}. \tag{5}$$

The occurrence of the nonpropagating part $i\gamma^+/2p^+$ makes the treatment of fermions in front-form field theories much more difficult, as it gives rise to integrals that are much more singular than the corresponding integrals in time-ordered or manifestly covariant formulations. In Sec. III the general case of spin $\frac{1}{2}$ particles is discussed. As an illustration a box diagram, describing two fermions exchanging scalar bosons, is reduced to a set of LCT-ordered diagrams.

The algorithm we propose demonstrates the equivalence of Feynman diagrams to sets of x^+-ordered diagrams in the case of scalar and spin-$\frac{1}{2}$ fields. (In a way, this is the reverse of Wick's theorem for time-ordered perturbation theory. The fact that the Cauchy problem with a null plane as initial surface is ill posed makes the Wick theorem in front-form dynamics a strictly formal result. Different interpretations have lead to different perturbative expansions [12,13].) The popular belief that massive fields do not have these problems is a misconception. The leading behavior of the fields near the light front is independent of the mass.

A brief discussion on the extension of our treatment to diagrams with several loops is given in Sec. IV.

In the course of our investigation we encountered several technical difficulties. They are discussed in Sec. V, where solutions are given too. In particular we argue that there is no problem concerning zero modes, if the p^- integrals are regularized properly, viz., using a regularization that preserves covariance. But it shows that Feynman diagrams give rise to terms in the perturbative expansion of the S matrix that act on $p^+ = 0$ states.

The next section (Sec. VI) is concerned with the many mathematical details that were left out from the preceding sections, lest the main line of argument be blurred.

We close with a discussion of our results and compare them to some of the literature on light-front field theory.

II. EQUIVALENCE

Before we proceed with the equivalence proof, we define what we mean by equivalence. By application of the Feynman rules as ordinarily understood, one obtains manifestly covariant expressions[2] for terms in the perturbative expansion of S-matrix elements, expressed in terms of four-momenta, masses, spins, and dynamical ingredients: coupling constants. Wick's theorem can be understood as asserting that the S-matrix elements could be calculated as well in time-dependent perturbation theory, and as giving us an algorithm to combine the terms found in the latter case into manifestly covariant expressions. Thus Wick's theorem establishes the equivalence of time-dependent ("old-fashioned") and covariant perturbation theory.

In this paper we use the word equivalence in a similar way: each term in covariant perturbation theory, a Feynman diagram, can be written as the sum of amplitudes that can be *interpreted* as terms in a LCT-ordered perturbation series. (In the interest of brevity, we will use the terminology LCT-ordered diagrams.) In fact, those amplitudes are expressed in momentum-energy-space quantities, but it is a straightforward matter to translate them into space-time language, thus justifying our terminology.

By taking Feynman diagrams as our point of departure, we avoid the problems of front-form quantization mentioned before. In addition, we also sidestep the problem of identifying the independent degrees of freedom and the determination of commutation relations between them for a constrained system.

The splitting of a Feynman diagram into LCT-ordered ones results in amplitudes of the form

$$V_\alpha \frac{1}{P^- - H_0} V_\beta \frac{1}{P^- - H_0} \cdots \frac{1}{P^- - H_0} V_\sigma \frac{1}{P^- - H_0} V_\omega. \tag{6}$$

Here, P^- plays the role of the "energy" variable, conju-

[2]Except for noncovariant gauge terms in a noncovariant gauge like the light-cone gauge.

gate to the light-cone time (LCT) x^+. H_0 is again the energy, but now expressed in terms of the kinematical components p^+ and $p_\perp$ of the momenta of the particles in the intermediate state between two interactions. The objects V are the vertices that correspond to the local interactions. As we will show, expressions of this form arise naturally upon integration of a Feynman diagram over the minus component of the integration variable. In general, a number of LCT -ordered diagrams are derived from a single Feynman diagram. This is directly analogous to old-fashioned perturbation theory, where $n!$ time-ordered diagrams sum up to one Feynman diagram with n vertices. However, there exists an important difference: in LCT-ordered theory there are less diagrams owing to the linearity of the denominator of the single-particle propagator in the p^- variable

$$\frac{1}{p^2-m^2+i\epsilon}=\frac{1}{2p^+[p^- - \frac{p_\perp^2+m^2-i\epsilon}{2p^+}]}. \tag{7}$$

Consequently, to every propagator there corresponds only one pole in p^- and its location in the complex p^- plane depends on the sign as well as the magnitude of p^+. This property, already alluded to by Dirac [1], allows us to pose the condition that in any state $p^+ > 0$. In the past the status of this so-called "spectrum condition" has remained somewhat unclear. We shall demonstrate that it follows directly from our splitting procedure and from a natural reinterpretation of amplitudes, quite similar to the reinterpretation of negative-energy states as states of positive energy of antiparticles in time-ordered perturbation theory. In fact, our reduction algorithm shows that the LCT-ordered diagrams have the property that the internal lines carry positive p^+ momentum only. Therefore a better terminology might be *spectrum property*, but we stick to the term spectrum condition, because it is commonly used. In case one would like to formulate diagram rules in LCT-ordered perturbation theory, one could use the spectrum condition as a limitation of all intermediate states to states where every particle has positive p^+ momentum.

The spectrum condition is intimately related to causality. When the causal single-particle propagator Eq. (7) is Fourier transformed, one finds that the sign of p^+ determines whether one can extend the integral over the p^- axis to an integral along a closed contour in the complex p^- plane by adding a semicircle at infinity for positive or negative $\mathrm{Im}p^-$: $p^+ > 0$ corresponds to positive x^+ evolution. States with positive energy go forward in time and states with negative energy go backward in time.

One can argue formally that the spectrum condition holds for all intermediate states. As a result of the completeness of the physical Hilbert space each state is a superposition of free states and thus has a positive p^+ momentum. Any particle in a free state with positive p^+ has positive energy and goes forward in time. The conservation of kinematical momentum $(p^+, p_\perp)$ restricts the creation of particles in a Hamiltonian formulation, which is not the case in the equal-time formulation. We will show that this property indeed holds for the LCT-ordered perturbative expansion.

This result seems rather obvious for spin-0 bosons, but, to our knowledge, its proof has never before been given. For spin-$\frac{1}{2}$ particles, there are complications due to the nonpropagating part $i\gamma^+/2p^+$ of the fermion propagator. These render the equivalence proof in this case more difficult.

There is an important point worth mentioning: the pole moves in the complex p^- plane as a function of p^+, and even crosses the real axis at infinity for $p^+ = 0$. This makes the propagator undefined as it stands. The crossing at infinity give rise to so-called "zero modes" which will be dealt with later (see Sec. V A).

A. Examples

As a pedagogical example we reduce the box diagram and the crossed-box diagram in ϕ^3 theory[3] to the associated LCT-ordered diagrams. This gives us the opportunity to show the working of the reduction algorithm in great detail. Later on we will give the general form of the algorithm.

1. Box diagram

The box diagram consists of four propagators (see Fig. 1):

$$FD_\Box = \int \frac{dk^+ d^2k_\perp}{(2\pi)^3} D_\Box,$$

$$D_\Box = \int \frac{dk^-}{2\pi} \frac{1}{(k_1^2-m^2+i\epsilon)(k_2^2-m^2+i\epsilon)(k_3^2-m^2+i\epsilon)(k_4^2-m^2+i\epsilon)}, \tag{8}$$

[3]The type of theory is not essential for the arguments, the presence of a loop is.

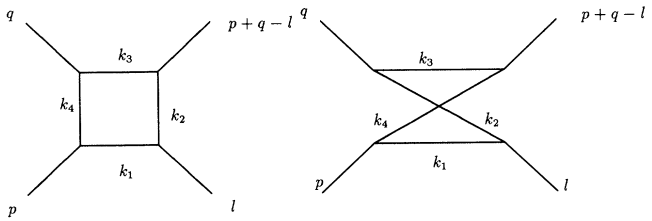

FIG. 1. Box and crossed-box diagrams.

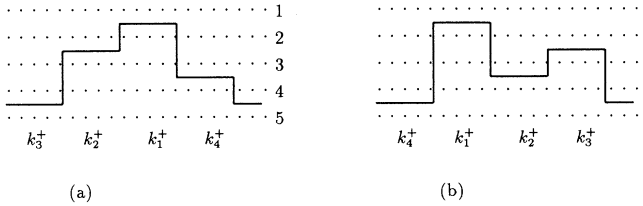

FIG. 2. The relative values of the longitudinal momenta, for the box diagram (a), and the crossed box diagram (b). All other box diagrams follow from these two through discrete symmetries. The absolute scale for the k_i^+'s is set by the value of k^+, the loop momentum.

with incoming momenta p and q and outgoing momenta l and $p+q-l$. The four momenta in the loop are $k_1 = k$, $k_2 = k-l$, $k_3 = k-p-q$, and $k_4 = k-p$. We can rewrite the integral in terms of energy denominators and phase space factors. We define the quantities $\{H_i\}_{i=1}^4$ as

$$H_1 = \frac{k_\perp^2 + m^2 - i\epsilon}{2k^+},$$
$$H_2 = l^- + \frac{(k_\perp - l_\perp)^2 + m^2 - i\epsilon}{2(k^+ - l^+)},$$
$$H_3 = p^- + q^- + \frac{(k_\perp - p_\perp - q_\perp)^2 + m^2 - i\epsilon}{2(k^+ - p^+ - q^+)},$$
$$H_4 = p^- + \frac{(k_\perp - p_\perp)^2 + m^2 - i\epsilon}{2(k^+ - p^+)}. \tag{9}$$

Then the k^- integral can be written as

$$D_\Box = \int \frac{dk^-}{2\pi\phi} \frac{1}{(k^- - H_1)(k^- - H_2)(k^- - H_3)(k^- - H_4)}. \tag{10}$$

The phase-space factor is given by $\phi = 16k^+(k^+ - l^+)(k^+ - p^+ - q^+)(k^+ - p^+)$.

The positions of the poles in the complex k^- plane depend on the values of the external momenta and the value of k^+. To calculate the time ordered diagram we must set the values of the external momenta p^+, q^+, and l^+. For specific values of k^+, the poles cross the axis and end up in the opposite half plane. When that happens, the integral changes discontinuously. The order in which the different poles cross the real axis depends on the values of the external momenta. In order to make our example definite, and without loss of generality, we assume $p^+ > l^+$. Then we have five regions on the k^+ axis:

1. $k^+ < 0$, $\mathrm{Im}H_i > 0$ $(i = 1,2,3,4)$;
2. $0 < k^+ < l^+$, $\mathrm{Im}H_1 < 0, \mathrm{Im}H_i > 0$ $(i = 2,3,4)$;
3. $l^+ < k^+ < p^+$, $\mathrm{Im}H_1, \mathrm{Im}H_2 < 0, \mathrm{Im}H_4, \mathrm{Im}H_3 > 0$;
4. $p^+ < k^+ < q^+ + p^+$, $\mathrm{Im}H_3 > 0, \mathrm{Im}H_i < 0$, $(i = 1,2,4)$;
5. $p^+ + q^+ < k^+$, $\mathrm{Im}H_i < 0$ $(i = 1,2,3,4)$

(see Fig. 2) with respectively zero, one, two, three, and four poles below the real axis. Each region corresponds with a different process in light-cone time. This observation leads naturally to the definition of a *skeleton graph.* Each physical region in k^+ corresponds to one skeleton graph. It is a graph that is topologically equivalent to the original Feyman diagram, but has its internal lines graded + or − corresponding to the signs of the $\mathrm{Im}H_i$, associated with the internal momenta k_i^μ.

In the first and the last case all the poles are at the same side of the real axis so the integral over k^- vanishes. Cases 2 and 4 are similar to each other. The integrals are calculated by closing the contour in the upper (lower) half plane of complex k^- values. The application of the residue theorem gives, for case 2,

$$D_\Box^2 = \frac{i}{\phi} \frac{1}{(H_4 - H_1)(H_3 - H_1)(H_2 - H_1)}, \tag{11}$$

and, for case 4,

$$D_\Box^4 = \frac{i}{\phi} \frac{1}{(H_3 - H_1)(H_3 - H_4)(H_3 - H_2)}. \tag{12}$$

Case 3 is the most interesting one. Straightforward application of the residue theorem gives the result

$$D_\Box^3 = \frac{-i}{\phi} \frac{(H_1 - H_2)(H_4 - H_3)(H_4 + H_3 - H_1 - H_2)}{(H_4 - H_1)(H_3 - H_1)(H_1 - H_2)(H_4 - H_3)(H_4 - H_2)(H_3 - H_2)}, \tag{13}$$

which can be split into two parts:

$$D_\Box^3 = -\frac{i}{\phi} \frac{1}{(H_4 - H_1)(H_4 - H_2)(H_3 - H_2)} - \frac{i}{\phi} \frac{1}{(H_4 - H_1)(H_3 - H_1)(H_3 - H_2)}. \tag{14}$$

A point to be clarified is the meaning of the denominators $(H_i - H_j)$. We choose the sign such that in these denominators $\mathrm{Im}H_i > 0$, corresponding to backward moving particles, while H_j has a negative imaginary part and refers therefore to forward moving particles.

Four-momentum conservation gives $k_4 = k_1 - p$. We set $k \equiv k_1$ and consider the case $\mathrm{Im}H_1 < 0$, $\mathrm{Im}H_4 > 0$, which means that $0 < k^+ < p^+$. Then, according to

the residue theorem, we have a factor $H_4 - H_1$ in the denominator corresponding to this diagram. This factor can be written as

$$H_4 - H_1 = p^- - \frac{(p_\perp - k_\perp)^2 + m^2}{2(p^+ - k^+)} - \frac{k_\perp^2 + m^2}{2k^+}. \quad (15)$$

The interpretation of the factor $H_4 - H_1$ is facilitated by cutting the diagram. We cut it first by a line cutting the legs of the loop with momenta k_1 and k_4 and all incoming lines except p. For every internal line, we define an on-shell value of the corresponding minus component as

$$k^-_{i,\mathrm{on}} = \frac{k_{i\perp}^2 + m^2}{2k_i^+}. \quad (16)$$

We define H_0 as the sum of the on-shell minus-momenta on the lines cut. In our example we find for the internal lines 1, 4 and the external line q,

$$H_0(1,4) = q^- + \frac{k_\perp^2 + m^2}{2k^+} + \frac{(p_{1\perp} - k_\perp)^2 + m^2}{2(p^+ - k^+)}. \quad (17)$$

The cutting line defines an intermediate state with total minus momentum $P^- = p^- + q^-$ and total on-shell minus momentum $H_0(1,4)$. The difference between these two is just $H_4 - H_1$, Eq. (15). Up till now, the direction of the internal four-momenta is determined by the direction in which the loop is passed. If we reverse the direction of k_4, the momentum with negative plus component, viz., $k^+ - p^+$ Eqs. (15), (16), is replaced by $p^+ - k^+$, which is then correctly interpreted as the plus component of the momentum of the particle corresponding to line 4.

If we consider a cut through k_1, k_3 and p, q, we will find $k_3 = k - p - q$. The same algebra that led to the result Eq. (17) will now give

$$\begin{aligned} P^- - H_0(1,3) &= p^- + q^- \\ &\quad - \left(\frac{k_\perp^2 + m^2}{2k^+} + \frac{(p+q-k)_\perp^2 + m^2}{2(p^+ + q^+ - k^+)} \right) \\ &= H_3 - H_1. \end{aligned} \quad (18)$$

It is clear that this procedure can be followed until the cut considered is cutting outgoing external lines only. There it stops. So, we conclude that we have the general result that any factor $(H_i - H_j)$ is equal to the difference of the minus component of the total momentum $P^- = p^- + q^-$, and the on-shell minus component of the momentum carried by the lines cut. Generally this holds for all combinations i and j such that $\mathrm{Im}H_i > 0$ and $\mathrm{Im}H_j < 0$ since the imaginary part is related to the sign of the on-shell momentum.

The LCT-ordered box diagrams can be interpreted as fourth order diagrams in LC-perturbation theory, having the form

$$V_4 \frac{1}{P^- - H_0} V_3 \frac{1}{P^- - H_0} V_2 \frac{1}{P^- - H_0} V_1. \quad (19)$$

In order to systematize the reduction of $D_\Box$ to a sum of residues that correspond to LCT-ordered diagrams, it is appropriate to consider both the algebraic structure and the connection of residues with diagrams.

First, we demonstrate the use of some concepts that will be of crucial importance for the proof of equivalence of the Feynman-diagram approach and LCT-ordered perturbation theory in the simple case of the box diagram. (The general proof is to be found in Sec. VI.)

The first object of interest is the Vandermonde determinant of order k:

$$\Delta(H_1, \cdots, H_k) = \begin{vmatrix} H_1^{k-1} & \cdots & H_1^2 & H_1 & 1 \\ \vdots & & \vdots & \vdots & \vdots \\ H_k^{k-1} & \cdots & H_k^2 & H_k & 1 \end{vmatrix}. \quad (20)$$

The second one is $W_{n,m}(H_1, \cdots, H_n | H_{n+1}, \cdots, H_{n+m})$ defined as

$$W_{n,m}(H_1, \cdots, H_n | H_{n+1}, \cdots, H_{n+m}) = (-1)^m \begin{vmatrix} H_1^{n+m-2} & \cdots & H_1^2 & H_1 & 0 & 1 \\ \vdots & & \vdots & \vdots & \vdots & \vdots \\ H_n^{n+m-2} & \cdots & H_n^2 & H_n & 0 & 1 \\ H_{n+1}^{n+m-2} & \cdots & H_{n+1}^2 & H_{n+1} & 1 & 0 \\ \vdots & & \vdots & \vdots & \vdots & \vdots \\ H_{n+m}^{n+m-2} & \cdots & H_{n+m}^2 & H_{n+m} & 1 & 0 \end{vmatrix}. \quad (21)$$

By direct computation one verifies easily the following statements:

$$\frac{W_{1,n}(y | x_1, \cdots, x_n)}{\Delta(y, x_1, \cdots, x_n)} = \frac{(-1)^n}{\prod_{i=1}^n (y - x_i)}, \quad (22)$$

$$\frac{W_{n,1}(x_1, \cdots, x_n | y)}{\Delta(x_1, \cdots, x_n, y)} = \frac{-1}{\prod_{i=1}^n (x_i - y)}. \quad (23)$$

Straightforward application of our rules gives for the skeleton graphs the following corresponding amplitudes:

$$D^2 = -\frac{i}{\phi} \frac{W_{3,1}(H_2, H_3, H_4 | H_1)}{\Delta(H_2, H_3, H_4, H_1)}, \quad (24)$$

$$D^4 = -\frac{i}{\phi} \frac{W_{1,3}(H_3 | H_1, H_2, H_4)}{\Delta(H_3, H_1, H_2, H_4)}. \quad (25)$$

In case 3 we have

$$D^3 = -\frac{i}{\phi}\frac{W_{2,2}(H_4,H_3|H_1,H_2)}{\Delta(H_4,H_3,H_1,H_2)}. \tag{26}$$

D^3 needs to be rewritten such that energy denominators appear. The energy denominator $(H_4 - H_1)^{-1}$ should appear in all LCT-ordered diagrams associated with D^3. It can be extracted as

$$\frac{W_{2,2}(H_4,H_3|H_1,H_2)}{\Delta(H_4,H_3,H_1,H_2)} = \frac{1}{(H_4-H_1)}\left(\frac{W_{1,2}(H_3|H_1,H_2)}{\Delta(H_3,H_1,H_2)} + \frac{W_{2,1}(H_4,H_3|H_2)}{\Delta(H_4,H_3,H_2)}\right) \tag{27}$$

and upon using Eq. (22) we recover the final expression (14). The proof in Sec. VI demonstrates how this type of reduction can be carried out in the general case.

Secondly, we describe the relation of this algebraic procedure with LCT-ordered diagrams. We begin with the Feynman diagram and enumerate the possible configurations of poles in the complex k^- plane. (Cases $1,\cdots,5$.) A pictorial representation of those cases where the contour integral over k^- does not vanish (cases 2, 3, and 4) is given by diagrams where the sign of ImH is indicated. (See Fig. 3.) The box diagram is relatively easy to reduce to LCT-ordered diagrams because in any associated skeleton graph there are at most two vertices that need to be ordered with respect to each other. There are only two internal lines which connect an incoming line with an outgoing line. Generally we call these kind of diagrams *flat*. The box diagram being flat, it does not show all the possible complications. Therefore, we also discuss the crossed box.

2. *Crossed box diagram*

The difference between the flat box and the crossed box is clearly visible in the sign patterns, for the imaginary parts of the denominators, one encounters when going around the loop. In the flat box one encounters the sign patterns $+--$, $++--$, and $+++-$. In the crossed box, however, the sign patterns are $+--$, $+-+-$, and $+++-$. When there are two poles on either side of the real k^-axis, two sign changes occur, which can be seen as "bends" in the internal line, from backward to forward and vice versa. The skeleton graphs with signatures $+--$ and $+++-$ are treated in the same way as the corresponding flat ones. The case $+-+-$ leads to four LCT orderings, which we explain now. There are two possible orderings of the two vertices with incoming external lines. Having chosen one ordering, we follow one of the internal lines until we reach a vertex with an outgoing external line. Either of the two vertices with outgoing lines can come first. This gives a total of four LCT ordered diagrams. The corresponding diagrams are depicted in Fig. 4. We choose again $p^+ > l^+$. The algebra for the $+-+-$ case, given by the interval $q^+ - l^+ < k^+ < l^+$, gives the residue

$$\frac{W_{2,2}(H_4,H_2|H_1,H_3)}{\Delta(H_4,H_2,H_1,H_3)} = \frac{1}{(H_4-H_1)}\left(\frac{W_{1,2}(H_2|H_1,H_3)}{\Delta(H_2,H_1,H_3)} + \frac{W_{2,1}(H_4,H_2|H_3)}{\Delta(H_4,H_2,H_3)}\right) \tag{28}$$

that can be reduced to

$$\frac{1}{(H_4-H_1)(H_2-H_3)(H_4-H_3)} + \frac{1}{(H_4-H_1)(H_2-H_3)(H_2-H_1)}. \tag{29}$$

In order to expose the four LCT-orderings, we write the two energy denominators next to the vertices with incoming lines as sums of two terms: e.g.,

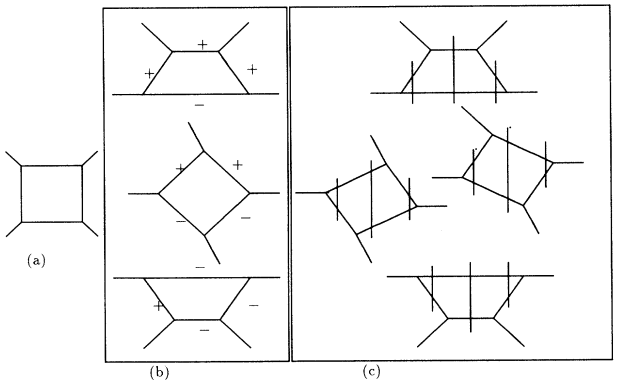

FIG. 3. The plane box. (a) Feynman diagram, (b) skeleton graphs, and (c) LCT-ordered diagrams.

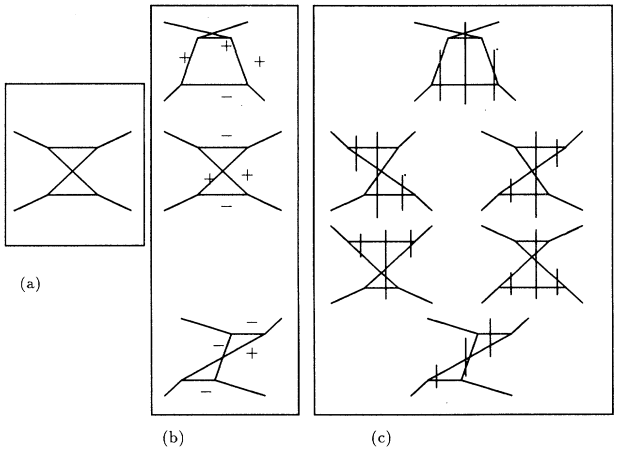

FIG. 4. The crossed box. (a) Feynman diagram, (b) skeleton graphs , and (c) LCT-ordered diagrams.

$$\frac{1}{(H_4-H_1)(H_2-H_3)}$$

$$= \frac{1}{(H_2-H_3)(H_4+H_2-H_3-H_1)} + \frac{1}{(H_4-H_1)(H_4+H_2-H_3-H_1)}. \quad (30)$$

Inserting these two denominators in the above expression gives four LCT-ordered diagrams:

$$D^2_\times = \frac{i}{\phi}\frac{1}{(H_2-H_3)(H_4+H_2-H_3-H_1)(H_4-H_3)},$$
$$D^3_\times = \frac{i}{\phi}\frac{1}{(H_4-H_1)(H_4+H_2-H_3-H_1)(H_4-H_3)},$$
$$D^4_\times = \frac{i}{\phi}\frac{1}{(H_2-H_3)(H_4+H_2-H_3-H_1)(H_2-H_1)},$$
$$D^5_\times = \frac{i}{\phi}\frac{1}{(H_4-H_1)(H_4+H_2-H_3-H_1)(H_1-H_2)}. \quad (31)$$

The LCT-ordered diagrams D^1 and D^6 are obtained in a similar way as in the case of the box diagram. Now we can easily answer the question why the number of LCT-ordered diagrams is smaller than the number of ordinary time-ordered diagrams. In the latter case, a loop with four vertices leads to 4! = 24 diagrams. For the LCT-ordered diagrams the number is reduced, because of the smaller number of poles. We can also interpret it as the *spectrum condition*. The spectrum condition restricts the plus component of any momentum on any line, internal as well as external, to non-negative values. Internal lines with negative plus momentum correspond to poles with positive imaginary part and are interpreted as antiparticles. By reversing the direction of the momenta on these internal lines while maintaining four-momentum conservation, these lines can be again associated with particles. So, conservation of plus momentum then provides the limitation of possible diagrams. The number of diagrams however, does depend on the external momenta; it is four in the case of the box diagram and six for the crossed box diagram.

B. General case

In a typical Feynman diagram on encounters several single-particle propagators. Following the same line of reasoning as used in the two examples given above, one will find that the corresponding poles in the loop variable k^- are located at different sides of the real k^- axis, depending on the value of k^+. To illustrate this fully general property, we consider a one-loop diagram with N vertices, N internal, and N external lines. The number of incoming lines is N_1; there are $N_2 = N - N_1$ outgoing lines. Suppose we call our integration variable k and identify it with k_N (see Fig. 5). Four-momentum conservation takes the form

$$k_i^\mu = k^\mu + K_i^\mu(p_1^\mu, ..., p_N^\mu), \quad (32)$$

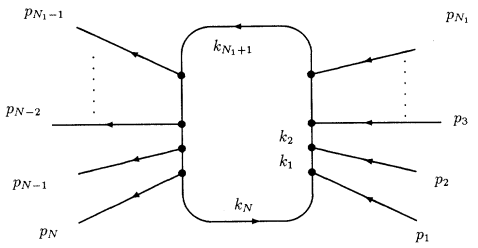

FIG. 5. One-loop diagram.

where the functions $K_i^\mu(p_1^\mu, ..., p_N^\mu)$ are linear. It is obvious that for arbitrary, but fixed external momenta all $k_i^+ < 0$ ($k_i^+ > 0$) for $k^+ \to \infty$ ($k^+ \to -\infty$). So, we can divide the real k^+ axis into different regions, a semi-infinite region where all $k_i^+ < 0$, another where all $k_i^+ > 0$, and $N-1$ finite regions where some of the k_i^+ are positive, the others being negative.

We will use here again the concept of a skeleton graph, as we did in the cases of the box and crossed box diagrams. For any Feynman diagram with given values of the external momenta, and for every interval in the loop variable k^+, one draws a graph that is topologically equivalent to the original Feynman diagram and has its internal lines graded either + or −, corresponding to the signs of the imaginary part of the poles H_i. In the one-loop case we thus find for $k^+ \to -\infty$ the skeleton graph with all lines graded +; there are $N-1$ skeleton graphs with lines graded + as well as lines graded − and, finally, for $k^+ \to \infty$, a skeleton graph with all lines graded −. From our discussion of the causal single-particle propagator it becomes immediately clear that lines graded − (+) correspond to particles moving forward (backward) in x^+ evolution. This justifies the terminology we adopt: if two vertices in a skeleton graph are connected by a line with internal momentum say $k_i^+ > 0$, then the vertex from which the momentum k_i^μ is flowing is said to be *earlier* than the vertex into which k_i^μ is flowing.

Apparently, each skeleton graph corresponds to a (partial) LCT ordering of the vertices in a Feynman diagram. The graphs with all lines graded + or all graded − correspond to a cyclic LCT ordering of the vertices that contradicts logic. Fortunately, these graphs are associated with the situation that all poles in k^- are lying at one side of the real k^- axis, in which case the amplitude vanishes. In all other graphs there is at least one vertex with an outgoing internal line with positive plus momentum and an incoming internal line with a negative plus momentum, and at least one vertex where the situation is reversed. The former vertices are called *early*, the latter *late* vertices. A sign change in the skeleton graph corresponds with an early or a late vertex, the other vertices are called *trivial* (see Fig. 6).

If only one early and one late vertex are present in a given skeleton graph, the partial ordering is complete after the trivial vertices are ordered. This was the case for the flat box diagram. Otherwise, the different early vertices must be ordered with respect to each other and with respect to the late vertices. This additional ordering

FIG. 6. The sign change in $\mathrm{Im}H_i$ correspond to early or late vertices. Both lines go in the same time direction. The sign of $\mathrm{Im}H_i$ is opposite to the sign of k_i^+.

produces several LCT ordered diagrams associated with a single skeleton graph. In this way, a single Feynman diagram gives rise to a number of consistently LCT ordered diagrams. At this stage one reverses the directions of the four-momenta k_i^μ on all those lines i where $k_i^+ < 0$. One sees immediately that as a result early vertices have only outgoing internal momenta, whereas late ones have only incoming internal momenta.

We use the late vertices in a different way than the early vertices. Starting from an early vertex, all vertices on the lines going out from this vertex are ordered relatively to this vertex. However, vertices lying on different lines are not yet ordered relative to each other. For two lines starting at different early vertices and connected at a late vertex, we can fix the relative ordering of the intermediate vertices, since all vertices on both lines must occur before the late vertex. When all late vertices have been encountered, their relative ordering determines the complete ordering of the full diagram.

The last point to be clarified is the form of the amplitudes corresponding to LCT ordered diagrams. We consider again the one-loop diagram and write the covariant amplitude as

$$FD = \int \frac{d^4k}{(2\pi)^4} \frac{1}{[k_1^2 - m_1^2 + i\epsilon]\cdots[k_N^2 - m_N^2 + i\epsilon]}, \quad (33)$$

where for the sake of simplicity we have put all vertex functions equal to unity. Using Eq. (32) we can write, for a typical factor in the denominator,

$$\begin{aligned} k_i^2 - m_i^2 + i\epsilon &= 2k_i^+\left(k_i^- - \frac{k_{i\perp}^2 + m_i^2 - i\epsilon}{2k_i^+}\right) \\ &= 2k_i^+\left(k^- + K_i^- - \frac{(k+K_i)_\perp^2 + m_i^2 - i\epsilon}{2k_i^+}\right) \\ &\equiv 2k_i^+(k^- - H_i). \end{aligned} \quad (34)$$

The poles in k^-, H_j, are functions of the kinematical components of k^μ and the external momenta p_j^μ. The imaginary part of H_i, $\mathrm{Im}H_i$, is determined by the sign of k_i^+. Now suppose that for given external momenta k^+ is such that m pole positions are located in the upper half plane ($\mathrm{Im}H_i > 0$) and $n = N - m$ in the lower half plane ($\mathrm{Im}H_j < 0$). In order to simplify the discussion, we renumber the lines such that $\mathrm{Im}H_i > 0$ for $1 \le i \le m$, $\mathrm{Im}H_j > 0$ for $m+1 \le j \le N = m+n$. Consider the k^- integral by itself:

$$D_{m,n} = \int \frac{dk^-}{2\pi 2^N k_1^+\cdots k_N^+} \frac{1}{[k^- - H_1]\cdots[k^- - H_N]}. \quad (35)$$

After performing the integration by closing the contour in either $\mathrm{Im}k^- > 0$ or $\mathrm{Im}k^- < 0$ one obtains a rational function of the H_i's:

$$D_{m,n} = \frac{i}{2^N k_1^+\cdots k_N^+} \frac{W_{m,n}(H_1,\cdots,H_m|H_{m+1}\cdots H_N)}{\Delta(H_1,\cdots,H_N)}. \quad (36)$$

Details on the functions $W_{m,n}$ and Δ are given in Sec. VI. As we argued before, the k^+ integration splits into $N+1$ intervals, $(-\infty, k^+(0)), (k^+(0), k^+(1)), \cdots, (k^+(N-1), +\infty)$, where the boundaries $k^+(i)$ are defined such that in the interval $(k^+(r-1), k^+(r))$ there are, for finite r, precisely r H_i's with $\mathrm{Im}H_i > 0$. In each of the finite intervals one skeleton graph is present corresponding to one k^- integral $D_{m,n}$. For either n or m different from 1, $D_{m,n}$ does not have the desired form Eq. (6). The full Feynman diagram is recovered by summing $D_{m,n}$ over m from 1 to $N-1$, integrating over k^+ over the appropiate finite interval, and over $k_\perp$. A further reduction, corresponding to the transition from the partially ordered skeleton graphs to the completely ordered diagrams must be performed. The heuristics that help us to do so is provided by the space-time concepts. Take any early vertex and identify it with an *event* at some LCT $x^+ = \tau_0$. Suppose H_1 and H_{m+1} are the poles corresponding to the outgoing and incoming internal lines, respectively, at this vertex. The intermediate state with momenta k_1 and k_{m+1} corresponds to the LC-energy denominator $H_1 - H_{m+1}$. We can convince ourselves that this is correct if the reversal of four-momenta on lines with $k_j^+ < 0$ is affected. We find

$$H_1 - H_{m+1} = P^- - \frac{k_{1\perp}^2 + m_1^2}{2k_1^+} - \frac{k_{m+1\perp}^2 + m_{m+1}^2}{2k_{m+1}^+}. \quad (37)$$

The identification of P^- becomes clear when one uses the surface τ to cut the internal and external lines. We can close the surface by cutting all the external lines attached to the piece of the Feynman diagram out of which the p^+ momentum flows. The momentum flow through this first cut plane τ_0 equals the flow through the second cut plane τ since energy momentum is conserved locally in a Feynman diagram. The flow of P^- through the internal lines equals the initial flow into the diagram minus the flow through the external lines cut at τ. The loop momenta do not contribute because they go into the τ cut plane as well as out of the cut plane, so there is no net contribution of these momenta. (We stress here that this interpretation is correct only after reversal of the four-momenta on the lines with $\mathrm{Im}H_j > 0$.) For brevity we call denominators of the form $H_i - H_j = P^- - H_0(i,j)$ *energy denominators*. These cut planes can be interpreted as equal-time surfaces. (See Fig. 7.)

Now the strategy is clear. For every skeleton graph one uses the surface $x^+ = \tau$ to cut lines that give rise to energy denominators. That this is possible is the content of our proof of equivalence. Indeed, as we demonstrate in Sec. VI, we have

$$\frac{W_{m,n}(H_1,\cdots,H_m|H_{m+1},\cdots,H_N)}{\Delta(H_1,\cdots,H_N)} = \frac{1}{H_1-H_{m+1}}\left(\frac{W_{m-1,n}(H_2,\cdots,H_m|H_{m+1},\cdots,H_N)}{\Delta(H_2,\cdots,H_m,H_{m+1},\cdots,H_N)} + \frac{W_{m,n-1}(H_1,\cdots,H_m|H_{m+2},\cdots,H_N)}{\Delta(H_1,\cdots,H_m,H_{m+2},\cdots,H_N)}\right). \tag{38}$$

That this identity leads to a recurrence follows from the fact that the two terms in the right-hand side (RHS) of Eq. (38) have the same form as the original one. The reduction stops if either n or m is reduced to 1.

There remains one loose end that we tie up now. If several early vertices occur, we have to consider all LCT orderings of them. (This happens if $n \geq 2$.) Moreover, we may have to consider LCT orderings such that some late vertices occur before some, but not all, early vertices. In all those cases the number of internal lines cut by an $x^+ = \tau$ surface is greater than 2, but always even: for every line going into this surface there is a corresponding outgoing line. We have seen that a pair of lines, one incoming, the other outgoing, that connect in an early (or late, for that matter) vertex, gives rise to an energy denominator, say $H_i - H_j$. When two pairs of such lines occur, there will be two energy denominators, which we call *simultaneous parts*. A simple example illustrates this. Let the two early vertices be α and β, and p_α^μ and p_β^μ the momenta on the two corresponding incoming external lines. The reduction algorithm gives two factors, one corresponding to the vertex α, of the form $1/(H_{i_\alpha} - H_{j_\alpha})$, the other being $1/(H_{i_\beta} - H_{j_\beta})$. As before, we can rewrite such factors, upon reversing the backward flowing momenta, in the form $1/[P^-(\beta) - H_0(\beta)]$ and $1/[P^-(\alpha) - H_0(\alpha)]$, where $P^-(\gamma), \gamma = \alpha, \beta$ is the total net external minus momentum flowing into vertex γ. A simple algebraic identity

$$\frac{1}{P^-(\alpha)-H_0(\alpha)}\frac{1}{P^-(\beta)-H_0(\beta)} = \frac{1}{P^-(\alpha)+P^-(\beta)-H_0(\alpha)-H_0(\beta)}\left(\frac{1}{P^-(\alpha)-H_0(\alpha)}+\frac{1}{P^-(\beta)-H_0(\beta)}\right) \tag{39}$$

combines the two factors in the correct way. The first factor can be rewritten as $1/[P^-(\alpha\cup\beta) - H_0(\alpha\cup\beta)]$, which we recognize as an energy denominator for the intermediate state with the four internal lines i_α, j_α, i_β, and j_β. The combination $1/[P^-(\alpha)-H_0(\alpha)][P^-(\alpha\cup\beta)-H_0(\alpha\cup\beta)]$ corresponds to the LCT-ordered diagram where the vertex α comes before vertex β, the other part of the RHS of Eq.(39) corresponding of course to vertex β preceding vertex α (see Fig. 8). Clearly, the splitting formula works also recursively, so it applies to any number of pairs of internal lines.

With this observation we end our general discussion of the reduction algorithm. We stress that the LCT-ordered language used here has heuristic value only, but does not replace a strict proof. The algebraic details are provided in Sec. VI.

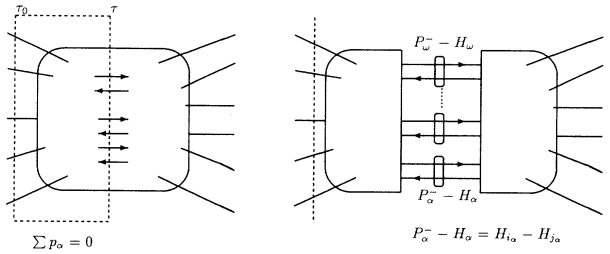

FIG. 7. Illustration of the cut procedure in a general n-leg diagram. For each cut area there is four-momentum conservation in a Feynman diagram. We can use this to make general statements for an intermediate state. The minus momentum transferred across the intermediate state is equal to the incoming minus momentum. The sum of energy denominators contains the sum of all external minus momenta minus the sum of all on-shell values of the particle lines. Loop momenta drop out because these go in and out of the cut area.

III. SPIN-$\frac{1}{2}$ PARTICLES

In the previous sections we dealt with scalar particles only, thus avoiding complications due to summations over spin degrees of freedom in intermediate states. Here, we discuss these complications for spin-$\frac{1}{2}$ particles. The reduction algorithm in this case is partly identical to the algorithm for scalar particles. However, we now have to include in our treatment not only the energy denominators, but also the numerators. Consider the Feynman propagator for a single particle. The spin sum $\not{p} + m$ depends on p^-, so we have to account for that when we define the skeleton graphs corresponding to a Feynman diagram. It has been argued before [12] that one can split the Feynman propagator into two pieces, one that is independent of p^-, the *instantaneous part*, and another piece, the *propagating part*, where p^- occurs in the denominator only:

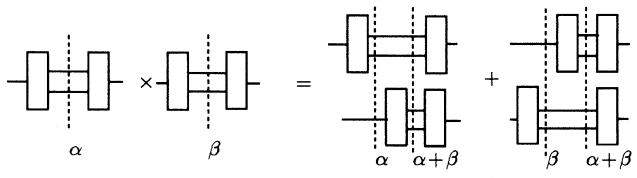

FIG. 8. The product of two time orderings is the sum of the relative orderings.

$$\frac{\not p + m}{p^2 - m^2 + i\epsilon} = \frac{p_{\rm on} + m}{p^2 - m^2 + i\epsilon} + \frac{\gamma^+}{2p^+} = \sum_\alpha \frac{u^{(\alpha)}(p) \otimes \bar u^{(\alpha)}(p)}{p^2 - m^2 + i\epsilon} + \frac{\gamma^+}{2p^+}, \qquad (40)$$

with the obvious definition $p^\mu_{\rm on} = (p^-_{\rm on}, p^+, p_\perp)$, where $p^-_{\rm on} = (p^2_\perp + m^2)/(2p^+)$. The spin sum $\sum_\alpha u^{(\alpha)}(p) \otimes \bar u^{(\alpha)}(p)$ runs over a complete basis in spin space, viz., particles and antiparticles.

In order to illustrate the differences between the purely scalar case and the situation where spin-$\frac{1}{2}$ particles occur, we discuss in the next subsection the flat box diagram with two bosons and two fermions.

A. Example: Fermion box diagram

Consider the case of two spin-$\frac{1}{2}$ fermions exchanging spinless bosons. A Feynman diagram for the fourth order in perturbation theory is shown in Fig. 9(a). The momenta are defined similar to the scalar case, Fig. 1. Before the associated skeleton graph can be drawn, one must split the fermion propagators for the intermediate states into the two parts: instantaneous and propagating. This results in four different diagrams shown in Fig. 9(b). In these four, the p^- dependence of the propagators is present in the denominators only. Therefore, one can apply the methods described in the previous section immediately, since the numerator does not depend on the integration variable. Doing so, one obtains the eight skeleton graphs drawn in panel (c). These graphs form the basis of the splitting into LCT-ordered diagrams. After this has been achieved one can combine certain diagrams into a single diagram by adding the propagating part to the instantaneous part of the fermion propagator. This regrouping of diagrams is represented graphically in the last panel of this figure. The formulas associated with the four final diagrams are

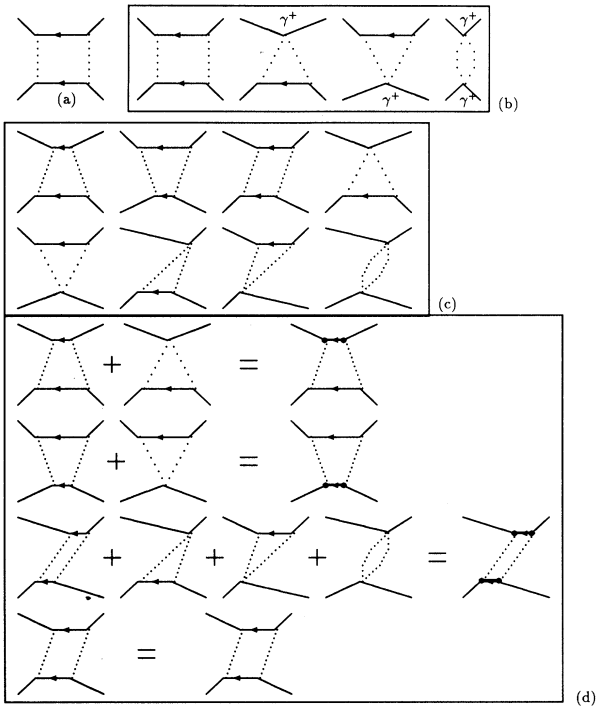

FIG. 9. (a) The Feynman diagram, (b) the corresponding diagrams with on-shell spinor projections or instantaneous parts, (c) the skeleton graphs, (only the tilted box leads to two LCT-ordered diagrams), and (d) the summed LCT-ordered diagrams, which yields the adjusted blink propagators.

$$\begin{aligned}
D^{(1)} &= \int \frac{dk^+ d^2k_\perp}{(2\pi)^3\phi} \frac{\gamma^a\Lambda_3\gamma^b \otimes \gamma^c\Lambda_1\gamma^d}{[P^- - H_0(1,4)][P^- - H_0(1,3)][P^- - H_0(1,2)]} \\
&\quad + \int \frac{dk^+ d^2k_\perp}{(2\pi)^3\phi} \frac{\gamma^a\gamma^+\gamma^b \otimes \gamma^c\Lambda_1\gamma^d}{[P^- - H_0(1,4)][P^- - H_0(1,2)]} \\
&= \int \frac{dk^+ d^2k_\perp}{(2\pi)^3\phi} \frac{\gamma^a\Omega_3\gamma^b \otimes \gamma^c\Lambda_1\gamma^d}{[P^- - H_0(1,4)][P^- - H_0(1,3)][P^- - H_0(1,2)]}, \\
D^{(2)} &= \int \frac{dk^+ d^2k_\perp}{(2\pi)^3\phi} \frac{\gamma^a\Lambda_3\gamma^b \otimes \gamma^c\Omega_1\gamma^d}{[P^- - H_0(1,4)][P^- - H_0(1,3)][P^- - H_0(2,3)]}, \\
D^{(3)} &= \int \frac{dk^+ d^2k_\perp}{(2\pi)^3\phi} \frac{\gamma^a\Omega_3\gamma^b \otimes \gamma^c\Omega_1\gamma^d}{[P^- - H_0(1,4)][P^- - H_0(2,4)][P^- - H_0(2,3)]}, \\
D^{(4)} &= \int \frac{dk^+ d^2k_\perp}{(2\pi)^3\phi} \frac{\gamma^a\Lambda_3\gamma^b \otimes \gamma^c\Lambda_1\gamma^d}{[P^- - H_0(1,4)][P^- - H_0(1,3)][P^- - H_0(2,3)]}.
\end{aligned} \qquad (41)$$

The objects Λ and Ω are defined as

$$\Lambda_i = \not k_{i,\rm on} + m_i, \qquad (42)$$

and

$$\Omega_i = \not k_i + m_i = \Lambda_i + \gamma^+(k_i^- - k^-_{\rm on}). \qquad (43)$$

The on-shell values of the minus components have been defined before; see Eq. (5). The energy denominator $P^- - H_0(1,2)$ is of course

$$P^- - H_0(1,2) = p^- + q^- - k^-_{1,\rm on} - k^-_{2,\rm on} - q^-_{\rm on} = p^- - \frac{k^2_{1\perp} + m_1^2}{2k_1^+} - \frac{k^2_{2\perp} + m_2^2}{2k_2^+}, \qquad (44)$$

and the other ones are defined similarly. The phase-space element ϕ has also been given before, below Eq. (10).

The flat fermion box shows clearly the peculiar complications caused by spin. Because the numerators and the denominators of the fermion propagators depend both linearly on the integration variable k^-, one has to perform a Laurent expansion in order to identify the pole terms. This leads to a number of "intermediate amplitudes," equal to 2^F, where F is the number of internal fermion lines. These amplitudes give rise to skeleton graphs that can be reduced to LCT-ordered diagrams in the, by now, familiar way. The LCT-ordered diagrams in which an element $\gamma^+/2k_i^+$ occurs are special, because associated to every one of them there occurs a diagram where the element $\gamma^+/2k_i^+$ is replaced by $\Lambda_i/[2k_i^+(P^- - H_0)]$. This happens only in those cases where the on-shell value $H_i = (k_i^2 + m_i)/2k_i^+$ occurs in a single energy denominator. These are the states that begin and end with the creation and the annihilation of the same particle. We call an internal line with this property a *blink*. In the case considered above, $D^{(1)}$ contains H_3 in only one factor in the denominator, the same holds for $D^{(2)}$ and H_1, whereas $D^{(3)}$ contains the blinks H_1 and H_3. If a blink occurs, one can recombine, after the LCT-ordering has been performed, the propagating part and the instantaneous part into a complete propagator. This is done in the diagrams $D^{(1)}$, $D^{(2)}$, and $D^{(3)}$ Eq. (41), and illustrated in Fig. 9(d), where the thick lines beginning and terminating in dots symbolize complete propagators.

B. Including the instantaneous terms

By now, it is relatively easy to formulate the general reduction algorithm. It has four steps:

(i) For a given Feynman diagram, perform the Laurent expansion of the fermion propagator, i.e., split the propagator into a propagating part and an instantaneous part; (ii) determine the skeleton graphs for all diagrams obtained in step (i); (iii) perform the reduction of all skeleton graphs in exactly the same way as it was done in the scalar case; (iv) identify the blinks and sum the diagrams corresponding to the same blink in order to obtain amplitudes with complete spin sums.

In order to understand why we recommend step (iv) we consider the general case. Let k_i^μ be the four-momentum of a blink. The two corresponding diagrams, partly shown in Fig. 10, contain the factors[4]

$$\begin{aligned} G_i &= \frac{1}{2k_i^+}\frac{\Lambda_i}{P^- - (\cdots H_i \cdots)}, \\ \Lambda_i &= \gamma^+ H_i + \gamma^- k_i^+ + \gamma_\perp \cdot k_\perp + m_i, \\ H_i &= (k_{i\perp}^2 + m_i)/2k_i^+, \\ g_i &= \gamma^+/2k_i^+. \end{aligned} \tag{45}$$

[4]We define $\gamma_\perp = (0, \gamma_1, \gamma_2, 0)$, $k_\perp = (0, k_1, k_2, 0)$, and $\gamma_\perp \cdot k_\perp = -(\gamma_1 k_1 + \gamma_2 k_2)$.

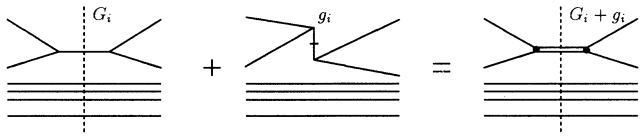

FIG. 10. The state begins and ends with the creation and annihilation of the same particle. The singularity in this diagram cancels against the same singularity in the instantaneous diagram.

We see that both G_i and g_i become singular at $k_i^+ = 0$. These two singularities appear to cancel. We can see this most clearly if we realize that the denominator $P^- - (\cdots H_i \cdots)$ can be rewritten as $k_i^- - H_i$. If $k_i^+ \to 0$, then $H_i \to \infty$, so we see that in this limit G_i behaves as follows:

$$G_i \overset{k_i^+ \to 0}{\sim} \frac{1}{2k_i^+}\frac{\gamma^+ H_i}{k_i^- - H_i} \sim -\frac{\gamma^+}{2k_i^+} = -g_i. \tag{46}$$

Therefore, the sum of the two contributions is finite for $k_i^+ \to 0$.

$$\begin{aligned} G_i + g_i &= \frac{1}{2k_i^+}\frac{\gamma^+ H_i + \gamma^- k_i^+ + \gamma_\perp \cdot k_\perp + m_i}{k_i^- - H_i} + \frac{\gamma^+}{2k_i^+} \\ &= \frac{\gamma^+ k_i^- + \gamma^- k_i^+ + \gamma_\perp \cdot k_\perp + m_i}{2k_i^+(k_i^- - H_i)} \\ &\overset{k_i^+ \to 0}{\sim} -\frac{\gamma^+ k_i^- + \gamma_\perp \cdot k_\perp + m_i}{k_{i\perp}^2 + m_i^2}. \end{aligned} \tag{47}$$

This expression appears *after* the integration of the energy variable. Then k_i^- is a function of the external variables only and represents the p^--flow through the intermediate state under consideration.

C. General case

We have seen that singularities in LCT-ordered diagrams cancel similar singularities in instantaneous terms. The instantaneous terms might contain other divergences that are cancelled by lower-order terms with additional instantaneous terms. The question remains whether this procedure ends, or whether we are left with terms which contain only instantaneous singularities that do not cancel each other. In the section on divergent contour integration we show that the proper treatment of the shift of poles to infinity removes all singularities from each residue. So after the recombination of terms we will not have a residual term in the form of instantaneous parts. Although we are not concerned with gauge theories explicitly, we note that most of these terms drop in a gauge theory with the (naive) light-cone gauge, and in theories with scalar and pseudoscalar coupling, due to $\gamma^+\gamma^+ = \gamma^+\gamma^5\gamma^+ = 0 = \gamma^+\gamma^i\gamma^+$.

IV. MULTILOOP DIAGRAMS

The extension of the reduction algorithm from Feynman diagrams with one loop to Feynman diagrams with several loops is not difficult, but there are some points that need to be clarified. The loop integrations can be done one after another since the structure of a LCT-ordered diagram is not essentially different from a Feynman diagram. We will illustrate the procedure with a simple example in the section below.

A. Two-loop diagram

We consider the scalar diagram with two loops, depicted in Fig. 11. The corresponding integral is

$$D=\int \frac{dq^-dk^-}{(2\pi)^2\phi}\frac{1}{(k^- - H_1)(k^- - H_2)(k^- + q^- - H_3)(q^- - H_4)(q^- - H_5)}, \tag{48}$$

where phase factor $\phi = 2^5 k^+(k^+ - p^+)(k^+ + q^+)q^+(q^+ + p^+)$ and the poles are given by:

$$\begin{aligned}
H_1 &= \frac{k_\perp^2 + m^2}{2k^+} - \frac{i\epsilon}{k^+},\\
H_2 &= p^- + \frac{(p_\perp - k_\perp)^2 + m^2}{2(k^+ - p^+)} - \frac{i\epsilon}{k^+ - p^+},\\
H_3 &= \frac{(k_\perp + q_\perp)^2 + m^2}{2(k^+ + q^+)} - \frac{i\epsilon}{k^+ + q^+},\\
H_4 &= -p^- + \frac{(q_\perp + p_\perp)^2 + m^2}{2(q^+ + p^+)} - \frac{i\epsilon}{q^+ + p^+},\\
H_5 &= \frac{q_\perp^2 + m^2}{2q^+} - \frac{i\epsilon}{q^+}.
\end{aligned} \tag{49}$$

There are twelve sectors in $k^+ \otimes q^+$ space corresponding to twelve skeleton graphs. These sectors are depicted in Fig. 12, where also the signatures of the skeleton graphs are shown. The amplitude D vanishes if either the integral over k^- or the one over q^- vanishes. The former happens if $\mathrm{Im}H_1, \mathrm{Im}H_2$ and $\mathrm{Im}H_3$ have the same sign, the latter if this happens for $\mathrm{Im}H_3, \mathrm{Im}H_4$ and $\mathrm{Im}H_5$. We read off from Fig. 12 that there are two sectors remaining, denoted as **I** and **II**. In sector **I** we have $H_1, H_3, H_4 < 0$ and $H_2, H_5 > 0$. The reduction algorithm gives the LCT-ordered diagram **I** of Fig. 13, with LCT ordering $a < b < c < d$. In sector **II** we have $H_1, H_4 < 0$ and $H_2, H_3, H_5 > 0$. The corresponding LCT ordering is $a < c < b < d$. The only difference between the two diagrams is the sign of $\mathrm{Im}H_3$, that is linked to the two different LCT orderings of the vertices b and c. For the sake of completeness we give the algebraic expressions for the two LCT ordered diagrams. Upon integration over k^- we obtain

$$\begin{aligned}
D_{\mathbf{I}} &= \frac{i}{2\pi}\int \frac{dq^-}{\phi}\frac{1}{(H_2 - H_1)(q^- + H_2 - H_3)(q^- - H_4)(q^- - H_5)},\\
D_{\mathbf{II}} &= \frac{i}{2\pi}\int \frac{dq^-}{\phi}\frac{1}{(H_2 - H_1)(q^- + H_1 - H_3)(q^- - H_4)(q^- - H_5)}.
\end{aligned} \tag{50}$$

The q^- integration is straightforward and gives the result

$$\begin{aligned}
D_{\mathbf{I}} &= \frac{1}{\phi}\frac{1}{(H_2 - H_1)(H_2 + H_4 - H_3)(H_4 - H_5)},\\
D_{\mathbf{II}} &= \frac{1}{\phi}\frac{1}{(H_2 - H_1)(-H_5 - H_1 + H_3)(H_4 - H_5)}.
\end{aligned} \tag{51}$$

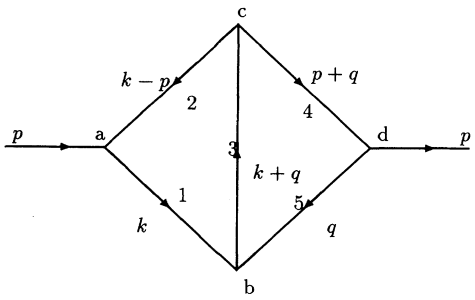

FIG. 11. The two-loop diagram.

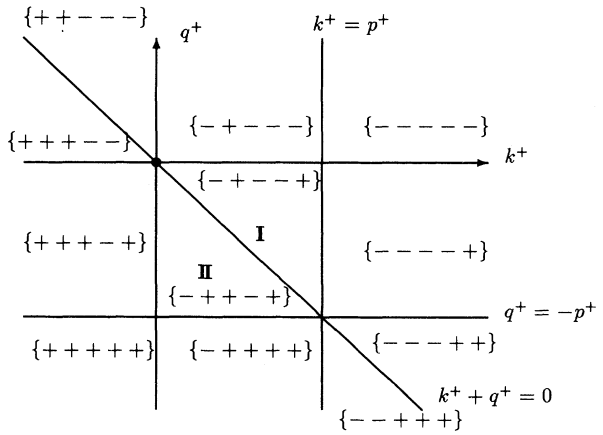

FIG. 12. The imaginary signs of $\{H_1, H_2, H_3, H_4, H_5\}$ for the different sectors in $k^+ \otimes q^+$ space. Only the inner regions **I** and **II** correspond to integrals and skeleton graphs.

After reversing the directions of the lines corresponding to negative k_i^+, viz., $k_2 = k - p$ and $k_5 = q$ in $D_{\rm I}$ and k_2, $k_3 = k + q$ and $k_4 = p + q$ in $D_{\rm II}$ we obtain the LCT-ordered diagrams depicted in Fig. 13. As before, every factor in the denominators of Eq. (51) can again be written in the form $P^- - H_0(i,j)$, where $H_0(i,j)$ is the sum of the energies on the lines i and j.

We see again that the integrations over k^+ and q^+ are limited to finite regions. After reversing the lines with negative $\mathrm{Im}H_i$, one sees that the diagrams obtained have the spectrum property.

B. General multiloop diagrams

In an arbitrary Feynman diagram with L loops, one must first identify the independent integration variables, say $q_1^-, \ldots, q_L^-$. Then one can characterize the different types of pole positions in an L-dimensional space with coordinates $(q_1^+, \ldots, q_L^+)$. The different signatures $(\mathrm{Im}H_1, \ldots, \mathrm{Im}H_N)$ divide this space into a number of sectors, each sector being associated with its particular skeleton graph. The sectors where the pole positions in all variables q_i^- are distributed over both half planes, $\mathrm{Im}q_i^- > 0$ and $\mathrm{Im}q_i^- < 0$, respectively, are necessarily finite. This is so, because for any loop i, all poles H_k occurring in this loop will have $\mathrm{Im}H_k < 0$ ($\mathrm{Im}H_k > 0$) if the integration variable q_i^+ goes to infinity (−infinity). Therefore, the sectors in $(q_1^+, \ldots, q_L^+)$ space which are semi-infinite in either of the q_i^+ do not contribute to at least one of the integrals over the q_i^- variables.

So, in general we will have a finite number of skeleton graphs that each gives rise to a finite number of LCT-ordered diagrams. Each and every one of them has the spectrum property. In the case of spin-$\frac{1}{2}$ particles, one can duplicate this algorithm, provided the full Feynman diagram, containing F fermion lines, is first split into 2^F intermediate diagrams according to the division of the spin-$\frac{1}{2}$ propagator into instantaneous and propagating parts. Then the reduction algorithm is applied to each of the intermediate diagrams, giving rise to the appropriate skeleton graphs and finally to the LCT-ordered diagrams, as was demonstrated in the one-loop case in the previous subsection. Of course, in the multiloop case blinks may occur as well as in the one-loop case. They are treated in exactly the same way as before. Thus we see that the multiloop Feyman diagrams, although algebraically more involved than the one-loop cases, can be reduced to LCT-ordered diagrams using precisely the same algorithm as was used for one-loop Feyman diagrams.

A final remark concerning the $i\epsilon$ prescription is in order here. It is used to define the deformed integration contours in all variables q_i^- simultaneously. After the residue theorem is applied to perform the contour integrations, the real parts of the poles are substituted in formulas like Eqs. (50, 51) ($\epsilon = 0$). If one would substitute complex poles in Eq. (50), ambiguities might arise in the values of the imaginary parts of the poles in q^-.

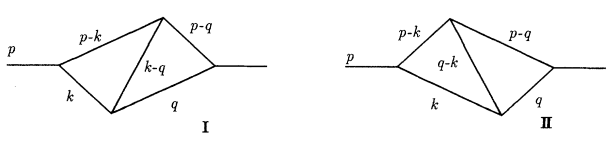

FIG. 13. The two LCT-ordered diagrams that follow from the two-loop diagram.

V. TECHNICAL DIFFICULTIES

In the previous sections we dealt with the equivalence between Feynman diagrams and LCT-ordered diagrams when the integration over k^- is well defined. There are two types of special cases were the k^- integration is not well defined. We can best illustrate these with simple examples. Consider a scalar loop like in ϕ^3 theory. If the external line has positive p^+ then the integration domain in k^+ is the interval $0 < k^+ < p^+$ [see Fig. 14(a)]. One may wonder what will happen if $p^+ = 0$, because in that case the measure of the integration interval is zero. The poles in the two propagators cross the real axis in the k^- plane for the same value of k^+: $k^+ = 0$. If this diagram is finite, there must occur a δ-like contribution in k^+. In cases where $p^2 \leq 0$, one can approach $p^+ = 0$ by performing a Lorentz-transformation (that, however, does not belong to the stability group of the null plane) and take the limit. Such a Lorentz-transformation is always possible for a spacelike external momentum, and there are situations where the momenta on three spacelike external lines can be transformed to have $p^+ = 0$ simultaneously. In other cases, like in (generalized) tadpoles, the measure of the integration domain is rigorously zero. We will consider a general approach which holds in all cases and give the same answer as a covariant calculation in the limit $p^+ = 0$. Tadpoles have a close relation with the ordering of operators in the Hamiltonian; therefore, we see that the $\delta(k^+)$ contributions have a relation with the ordering.

The other case where the k^- integration is ill defined, occurs if at most one pole is present in the k^- integration. This happens for all Feynman diagrams with at most one boson propagator and at least one fermion propagator in the loop. Then the intermediate diagrams with an instantaneous part of the fermion propagator combined with a boson propagator needs regularization. Other examples are diagrams with at least two instantaneous terms,

FIG. 14. Two cases where the energy integral is ambiguous: (a) if the k^+ momentum along the loop is constant; (b) if there is one pole left in the k^- integration; the pole of the boson accompanied by the instantaneous part of the fermion propagator.

which also lead to divergent integrals. The first order correction to the fermion self-energy in a theory of scalar bosons and fermions with Yukawa coupling, is a simple example [see Fig. 14(b)]. The fermion propagator has an instantaneous part such that the only k^- dependence of the integrand resides in the boson propagator. This integral is not defined, so we need a way to deal with this type of integrals in a consistent way. We are primarily interested in a treatment which does not interfere with the algebraic rules, so the regularization must be a linear operation. In addition we require it to be homogeneous in the integration variables. In both cases, one where tadpoles are present and the other where instantaneous parts give rise to infinities, we are lead by covariance in our choice of regularization. Other arguments do not restrict the regularization to a unique method, while covariance does.

A. "Zero modes" from energy integration

One of the integrals which shows the presence of zero modes in a time-ordered formulation has been discussed already by Yan [14]:

$$\lim_{k^+\to 0}\int dp^- \frac{1}{[2(p^+-k^+)p^- - m^2 + i\epsilon](2p^+p^- - m^2 + i\epsilon)}$$

$$= \int dp^- \frac{1}{(2p^+p^- - m^2 + i\epsilon)^2} \overset{\text{covariant}}{=} \frac{i\pi\delta(p^+)}{m^2} . \quad (52)$$

For $p^+ \neq 0$ there is one double pole either above or below the real axis so it was concluded that, since $p^+ = 0$ is an unphysical value (no free state can acquire $p^+ = 0$), the integral should vanish. A careful analysis shows that Eq. (52) is an ambiguous expression, so one can get any value (including the covariant answer) and one needs to choose a regularization to get a well-defined integral. (The proper covariant value was obtained by Yan by taking the limits $p^+ \downarrow 0$ and $p^+ \uparrow 0$ in a special way.)

For $p^+ = 0$ the p^- integral diverges, so ($p^+ \to 0, p^- \to \infty$) is the ambiguous point. If p^+ moves along the real axis and crosses $p^+ = 0$, the poles move through infinity and end up on the other side of the real axis. To deal with all singularities of this type at the same time, we introduce the variable $u = 1/p^-$ and study a general case:

$$D_n = \int dp^- \frac{1}{(2p_1^+p^- - H_1^\perp + i\epsilon)(2p_2^+p^- - H_2^\perp + i\epsilon)\cdots(2p_n^+p^- - H_n^\perp + i\epsilon)}$$
$$= \int du \frac{u^{n-2}}{[2p_1^+ - (H_1^\perp - i\epsilon)u]\cdots[2p_n^+ - (H_n^\perp - i\epsilon)u]} . \quad (53)$$

The integrand goes to zero like u^{-2} for $u \to \pm\infty$, therefore the integral is well defined, unless the integrand has a singularity at $u = 0$. So the only divergence can occur if $u \to 0$ which gives a finite contribution only if all p^+ momenta vanish at the same time. The poles in the variable p^- that moved to infinity, now correspond to poles in the variable u that cross the real axis at $u = 0$ when either of the variables p_i^+ is zero. If all p_i^+ happen to be equal, the integrand is singular at $u = 0$. [The first example, Eq. (52), is the special case with $n = 2; H_1^\perp = H_2^\perp = m^2$.] This gives a finite contribution to the integral of D over p^+, on support $p^+ = 0$, thus D contains a δ function in p^+.

The u coordinate regularization replaces all other arguments we might have to deal with this "zero-mode" problem. The choice of regularization determines the integral uniquely. Instead of treating the general expression, Eq. (53), we regularize the case of a single pole in the integrand and use an algebraic relation to obtain the general expression. Consider the integral

$$D_1 = \int du \frac{1}{u[2p^+ - (H^\perp - i\epsilon)u]} . \quad (54)$$

This expression is ambiguous for two reasons: it has a pole at $u = 0$ and a double pole occurring for $p^+ = 0 \wedge u = 0$. The first ambiguity we remove by adding a small imaginary part to one factor u coming from the Jacobian. In order to obtain a covariant expression we must do this symmetrically:

$$\frac{1}{u} \to \frac{1}{2}\left(\frac{1}{u + i\delta} + \frac{1}{u - i\delta}\right) . \quad (55)$$

We split the integral into two pieces; one just above the real axis and the other just below it. We do not give the singularities some strict nature (such as a principal value), which would lead to the square of the principal value for u^{-2}. Generally we treat the energy as a complex variable (since each pole corresponds to a particle), and the kinematical variables are treated geometrically. The choice Eq. (55) separates $p^+ > 0$ from $p^+ < 0$ for all positive values of ϵ and δ. Thus we find, for the regularized integral,

$$D_1^{\text{reg}} = \int du \frac{1}{2}\left(\frac{1}{u + i\delta} + \frac{1}{u - i\delta}\right) \frac{1}{[2p^+ - (H^\perp - i\epsilon)u]}$$
$$= -\frac{\pi i\theta(p^+)}{2p^+ + i(H^\perp - i\epsilon)\delta} + \frac{\pi i\theta(-p^+)}{2p^+ - i(H^\perp - i\epsilon)\delta}$$
$$= -\frac{2\pi i\theta(p^+)}{2p^+ + i(H^\perp - i\epsilon)\delta} . \quad (56)$$

For $p^+ < 0$ we reversed its sign to obtain the last line. Integrating D_1^{reg} over p^+ from 0 to a cutoff Λ and taking the limit $\epsilon \to 0$, gives $\pi[\ln(H^\perp) + \ln\delta + \pi i/2 - \ln 2\Lambda]$. We shall see that the constant part $\ln\delta + i\pi/2 - \ln 2\Lambda$ drops if we have two or more energy denominators. Using the algebraic relation

$$\frac{1}{\prod_{j=1}^{n}(2p^+p^- - H_i^\perp + i\epsilon)}$$

$$= \sum_{k=1}^{n} \frac{1}{(2p^+p^- - H_k^\perp + i\epsilon)\prod_{j\neq k}(H_k^\perp - H_j^\perp)} \quad (57)$$

the regularized integral becomes

$$\int\!\!\!\!\!\!-\, dp^- \frac{1}{(2p^+p^- - H_1^\perp + i\epsilon)\cdots(2p^+p^- - H_n^\perp + i\epsilon)}$$

$$= \sum_{k=1}^{n} \frac{i\pi\delta(p^+)\ln(H_k^\perp)}{\prod_{j\neq k}(H_k^\perp - H_j^\perp)} \,. \quad (58)$$

The function $\delta(p^+)$ appears here, because the integral is strictly zero for $p^+ \neq 0$, although integration over p^+ gives a finite result. The result Eq. (58) can also be obtained as a limiting case of Eq. (53) in the simultaneous limits $p_i^+ \to p^+, \forall i$. One can check that Eq. (58) is the same as the covariant result, using a Wick rotation such that $2p^+p^- - p_\perp^2 \to -|p|^2$. The limit for $H_i \to H_j$ is well-defined. The constant term has dropped since

$$\sum_{k=1}^{n} \frac{1}{\prod_{j\neq k}(H_k^\perp - H_j^\perp)} = 0 \,, \quad (59)$$

which follows from the fundamental theorem of algebra.

We emphasize here that these zero modes appear in loops where the p^+ momentum is constant along the loop. Zero modes can be interpreted as an infinite number of states (around $p^+ = 0$) which are infinitely off shell ($p_{\rm on}^- = \infty$), and thus have zero probability for propagation over a finite distance. The combination of both gives a finite contribution. This is reminiscent of the ultraviolet divergences, where the large number of high-energy states give an infinite contribution.

Although zero modes are needed to obtain the covariant answer, they remain slightly artificial, which can be seen from the configurations were they occur. It seems that nature is telling us that the high density of states for high energy causes trouble: divergent integrals appear which have to be regularized, and zero modes. Both result from singularities on the light cone.

B. Divergences in the fermion loop

In the section on diagrams containing fermions we stated that they could be reduced to LCT-ordered diagrams, provided no additional singularities would occur. In this section we deal with these singularities. We state that the regularization proposed here removes all of them. There remains one point to clarify: i.e., whether the method of regularization does indeed produce a covariant result. The latter point, however, will not be discussed in this paper.

We now have the tools to deal with the singularities in the fermion loop. Earlier (Sec. III) we saw that a blink combines two singular terms in such a way that we get a nonsingular expression. However, in general the low-order terms, with several instantaneous contributions, are singular by themselves. We will show that the contribution from the contour at infinity leads to these singularities. After subtraction of the latter the singularities are gone and a proper recombination of terms will remove apparent singularities.

For Feynman diagrams with at most one boson propagator in a loop there are singular parts in the contour integration. Even if the diagram would be convergent in the ordinary sense, i.e., in the covariant or instant form, it will still be divergent in k^- integration. The singular behavior of the fermion propagator on the light front is to blame.

Also in the case of bosons an ambiguity occurred (see Sec. V A). The result did depend on whether the contour was closed in the lower half plane or in the upper half plane. This problem could be resolved by choosing a particular combination of contours. We considered two contours, one consisting of the real axis and a semicircle in the upper half plane, the other one has the semicircle in the lower half plane. The integral over the real k^- axis was replaced by the average of the integrals over these two contours. This regularization turned out to have a number of desirable properties.

In the case of fermion loops the problem is more complex. A straightforward application of the residue theorem gives results that depends strongly on the choice of the contour. The integral is also more divergent than one would expect from naive power counting, and has noncovariant singularities. At the origin of these problems lies the contribution of the (semi) circle at infinity to the contour integral. We have to subtract this contribution. In a sense we propose a regularization of the contour integral.

For an integral that converges on the real axis, it does not matter whether we close the contour in the upper or the lower half plane. This means that the sum of all residues is zero:

$$\sum_i \mathrm{Res}_i = 0. \quad (60)$$

If the integration is divergent we have contributions at infinity, which add differently to the two contours (see Fig. 15). Therefore the two contours give different results. We denote this difference by Γ_∞. Then we have

$$\sum_i \mathrm{Res}_i = \Gamma_\infty. \quad (61)$$

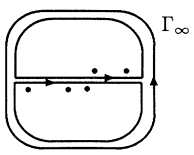

FIG. 15. The difference between the upper-plane contour and the lower-plane contour is the contour at infinity Γ_∞.

To solve this problem we "regularize" the residues by subtracting fractions of Γ_∞ from them:

$$\sum_i \mathrm{Res}_i^{\mathrm{reg}} = \sum_i (\mathrm{Res}_i - \alpha_i \Gamma_\infty) = 0, \qquad \sum_i \alpha_i = 1. \quad (62)$$

We then find the desired result that closing the contour in the upper half plane gives the same result as closing it in the lower half plane. We will see that the α_i's can be chosen such that the singularities cancel.

The k^- integral corresponding to a general Feynman diagram with a fermion loop can be written as

$$D_n = \int \frac{dk^-}{2^n k_1^+ \cdots k_n^+} \frac{(\gamma^+ k^- + \beta_n) \cdots (\gamma^+ k^- + \beta_n)}{(k^- - H_1) \cdots (k^- - H_n)}. \quad (63)$$

We wrote only the structure that depends on k^- and k^+ explicitly. We can consider one residue at a time, since the singularities of one residue are not canceled by another residue. The residue of the pole $(k^- - H_j)^{-1}$, and the contribution of the contour at infinity are

$$\mathrm{Res}_j = \frac{1}{2^n k_1^+ \cdots k_n^+} \frac{(\gamma^+ H_j + \beta_1) \cdots (\gamma^+ H_j + \beta_n)}{(H_j - H_1) \cdots (H_j - H_n)}, \quad (64)$$

$$\Gamma_\infty = \frac{1}{2^n k_1^+ \cdots k_n^+} \left[\left(\sum_{i=1}^n H_i \right) (\gamma^+ \cdots \gamma^+) + (\beta_1 \cdots \gamma^+) + \cdots + (\gamma^+ \cdots \beta_n) \right]. \quad (65)$$

The latter can best be calculated by changing the integration variable to $u = (k^-)^{-1}$ and integrating over a circle around the origin with a small radius, $|u| = \epsilon$. The residue Res_j has only singularities if $k_j^+ \to 0$, since then $H_j \to \infty$. In the limit $k_j^+ \to 0$ only a few terms survive. The surviving structure is precisely the contribution from the contour at infinity, which is independent of j:

$$\lim_{k_j^+ \to 0} \mathrm{Res}_j = \Gamma_\infty . \quad (66)$$

If we decompose the contribution from the contour at infinity now in such a way that each term contains only one singular point ($k_j^+ \to 0$), we can subtract these terms from the residues with the same singularities, and the resulting regularized residues are finite. If we define the quantities q_j^+ and $H_j^\perp$ as follows: $k_j^+ = k^+ - q_j^+$ and $H_j^\perp = 2k_j^+ H_j$, then we find that the following regularized residues are finite for $k_j^+ \to 0$:

$$\mathrm{Res}_j^{\mathrm{reg}} = \mathrm{Res}_j - \left(\frac{1}{2^n (k^+ - q_j^+) \prod (q_j^+ - q_i^+)} H_j + \sum_l \frac{H_l^\perp}{2^{n+1} (k^+ - q_j^+)(q_j^+ - q_l^+) \prod (q_j^+ - q_i^+)} + \frac{H_j}{2^n (q_j^+ - q_l^+) \prod (q_l^+ - q_i^+)} \right) (\gamma^+ \cdots \gamma^+) + \frac{1}{2^n (k^+ - q_j^+) \prod (q_j^+ - q_i^+)} [(\beta_1 \cdots \gamma^+) + \cdots + (\gamma^+ \cdots \beta_n)]. \quad (67)$$

Since each residue is now regular we know that there is a combination of LCT-ordered diagrams where each term is convergent. The blink procedure tells us how to do this step by step. The argument above tells us that there are no singularities left.

We killed two birds with one stone: we resolved the ambiguity in the contour integration and removed the singularities. These two problems are intimately related since the singularity comes from the pinching of the contour at infinity between the "pole at infinity" and an ordinary pole.

Another advantage of this procedure is that only the physical sectors are nonzero, a property that would be destroyed by ordinary contour integration. It allows us to keep a simpler view of causality and unitarity, where each line is associated with a particle moving forward in LC-time. In nonphysical sectors all the poles are on the same side of the axis. Then formula (62) tells us that the result is zero. We do not know whether this regularization leads to the same amplitude as the covariant calculations.

Example: Vacuum polarization

We will illustrate the procedure from the previous section with an example. The simplest diagram is the vacuum polarization diagram; a closed fermion loop with two fermion propagators:

$$D^{\mu\nu} = \int \frac{dk^-}{2\pi i} \frac{Tr[\gamma^\mu (\gamma^+ k^- + \beta_1) \gamma^\nu (\gamma^+ k^- + \beta_2)]}{4k_1^+ k_2^+ (k^- - H_1)(k^- - H_2)}. \quad (68)$$

We deal with the physical sector so we can assume, without loss of generality, $\mathrm{Im} H_1 > 0$ and $\mathrm{Im} H_2 < 0$. The result depends on the way the contour is closed. We will close the contour in the upper half plane. In terms of LCT-ordered diagrams we have the ordinary diagram, with two propagating fermions, and the diagram with the instantaneous part associated with the pole H_2 in the lower half plane. Together they give the residue of the pole H_1, as expected.

$$D_1^{\mu\nu} = \frac{\mathrm{Tr}[\gamma^\mu (\gamma^+ H_1 + \beta_1) \gamma^\nu (\gamma^+ H_1 + \beta_2)]}{4k_1^+ k_2^+ (H_1 - H_2)}. \quad (69)$$

If we would have chosen to close the contour in the lower half plane the result would be different. The difference is the result of a finite contribution of the semicircles. We still have to subtract the fraction of the contour at infinity which is given by (67):

$$\alpha_1\Gamma_\infty = \frac{\mathrm{Tr}[\gamma^\mu\gamma^+\gamma^\nu\gamma^+]}{4k_1^+(k_2^+-k_1^+)}\left(H_1+\frac{k_2^+H_2}{k_2^+-k_1^+}+\frac{k_1^+H_1}{k_1^+-k_2^+}\right)+\frac{\mathrm{Tr}[\gamma^\mu\beta_1\gamma^\nu\gamma^+]}{4k_1^+(k_2^+-k_1^+)}+\frac{\mathrm{Tr}[\gamma^\mu\gamma^+\gamma^\nu\beta_2]}{4k_1^+(k_2^+-k_1^+)}. \tag{70}$$

The LCT-ordered diagram obtained has no singularities, and is independent of the direction in which the contour is closed, since it is symmetric in H_1 and H_2:

$$D_1^{\mu\nu}-\alpha_1\Gamma_\infty = D_{\mathrm{reg}}^{\mu\nu} = \frac{\mathrm{Tr}\left[\gamma^\mu\left(\left(\frac{k_2^+H_2-k_1^+H_1}{k_2^+-k_1^+}\right)\gamma^++\beta_1\right)\gamma^\nu\left(\left(\frac{k_2^+H_2-k_1^+H_1}{k_2^+-k_1^+}\right)\gamma^++\beta_2\right)\right]}{4k_1^+k_2^+(H_1-H_2)}. \tag{71}$$

This result could not be obtained if we would have taken a combination of an upper-plane semicircle and a lower-plane semicircle; this would give a singular, and thus an ambiguous, result. The contribution of the contour at infinity should be decomposed in a unique way to obtain a regular expression.

We will not calculate the amplitude here since the diagram is divergent and the comparison is with other results is spoiled by renormalization. After this regularization the k^+ integration is automatically finite, since the domain is finite and the integrand is regular.

C. Dynamical spin

In a Hamiltonian theory we separate kinematical variables from dynamical ones. Starting from one equal-LCT surface, we evolve in the time direction to the next equal-LCT surface. In a covariant formulation, different interaction points could be on the same equal-LCT surface. Constraints should, in a Hamiltonian formulation, account for these parts. A straightforward interpretation does not exist; the constraints "evolve" with the order in perturbation theory, and so does the physical Hilbert space (constraints are working on the Hilbert space). We will illustrate this point with a Hilbert-space interpretation of the instantaneous interaction $\gamma^+/2p^+$.

The $(p^+)^{-1}$ singularity is ambiguous as it stands. We need a way to look at this part such that we avoid additional divergences which seem to appear. Note that the spinor-matrix elements of γ^+ are the same as those of p^+. Therefore we might suspect that the occurrence of γ^+ suppresses the singularity. To make this apparent we use the completeness of the physical Hilbert space. The physical Hilbert space is spanned by the free states. Therefore we can write the identity operator as the sum over all states:

$$\mathbb{1} = \sum_\alpha \int d^3p\ |u^{(\alpha)}(p)\rangle\langle u^{(\alpha)}(p)|. \tag{72}$$

We use this abstract notation because we don't want to bother with conventions which are not relevant. The normalization follows from the idempotency of the identity operator ($\mathbb{1}\cdot\mathbb{1}=\mathbb{1}$):

$$\begin{aligned}\langle u^{(\alpha)}(p)|u^{(\beta)}(p')\rangle &= \bar{u}^{(\alpha)}(p)u^{(\beta)}(p')\langle p|p'\rangle \\ &= \delta^{\alpha\beta}\delta^3(p-p').\end{aligned} \tag{73}$$

We can project $\gamma^+/(2p^+)$ onto the physical states by applying the identity operator on both sides:

$$\begin{aligned}\mathbb{1}\cdot\frac{\gamma^+}{2p^+}\cdot\mathbb{1} &= \sum_{\alpha\beta}\int d^3p'd^3p|u^{(\alpha)}(p')\rangle\langle u^{(\alpha)}(p')|\frac{\gamma^+}{2p^+}|u^{(\beta)}(p)\rangle\langle u^{(\beta)}(p)| \\ &= \sum_{\alpha\beta}\int d^3p'd^3p|u^{(\alpha)}(p')\rangle\delta^{\alpha\beta}\frac{\delta^3(p-p')}{2m}\langle u^{(\beta)}(p)| = \frac{\mathbb{1}}{2m}.\end{aligned} \tag{74}$$

There is no mixing between upper and lower components because they are spectrally separated:

$$\mathbb{1} = \left(\frac{\not{p}+m}{2m}+\frac{-\not{p}+m}{2m}\right)\theta(p^+). \tag{75}$$

Wherever $\gamma^+/(2p^+)$ appears we can replace it by $1/(2m)$, since Eq. (74) is an operator identity on our space. The instantaneous interaction can be interpreted as nothing but a point interaction, $1/(2p^+)$ being the phase space that goes with it and γ^+ the vertex.

However, these arguments do not hold in a Feynman diagram. The spin plays a dynamical role. In contrast to the instant-form dynamics, where all components of the angular momentum are kinematical, in front-form dynamics only the z component of the spin is a kinematical operator. The other components are involved in the interactions. It turns out that we can combine the $\gamma^+/(2p^+)$ singularity with the $1/p^+$ singularity that appears in a corresponding LCT-ordered diagram with a propagating fermion line, such that the singularities of the two cancel. Thus we find that in a Hamiltonian approach to light-front field theory, there is an intimate interplay between the singularities of the propagators and a singular piece of the interaction. Interestingly enough, this piece occurs even for free particles. In old-fashioned

ordinary time-ordered perturbation theory, i.e., instant form dynamics, the amplitude of propagation depends on the off-shell energy only, not on the polarization.

D. Analyticity and covariance

A Feynman amplitude is an analytical function of scalar objects like p_i^2, $p_i \cdot p_j$. Often, the real values of the scalars are the boundary values of the complex domain on which this function is defined. We use these arguments in order to be able to apply the residue theorem to integration over the loop variables and to perform Fourier transformations. All contour integrals are finite (if we do not pinch the contour) and coincide for integrals convergent on the real axis with the integral along this axis. (A coordinate transformation $y = x^{-1}$, as used in the section on zero modes, doesn't alter the results, since it maps the real axis on the real axis.) We cannot use the exponential e^{ikx} to improve the convergent along the semicircle of the contour (Jordan's lemma).

If we integrate over one coordinate separately, manifest covariance is lost. In the case of integration over ordinary energy this was not much of a problem since we can consider $\vec{p}^2 + m^2$ as real and then analyticity in p^0 is directly related to analyticity in $p_\mu p^\mu$. In light-front coordinates the situation is more complicated since $p^2 - m^2 = 2p^-p^+ - (p_\perp^2 + m^2)$. For real values of the scalar object the complex values of p^- and p^+ are related $[(p_\perp^2 + m^2)$ is real]. The coordinates are each others complex conjugate. After Wick rotation ($p^0 \to -ip^0$) this remains almost exactly true: $p^+ \to p$, $p^- \to -\bar{p}$. For a strip along the real axis we have $p^-\mathrm{Im}p^+ = -p^+\mathrm{Im}p^-$. Singularities that occur in a complex function can be regularized, but the relation between the conjugate variables restricts the possibilities of regularization. Singularities of an integer order (like $1/x$) cannot be integrated by parts. But one can approach these singularities in parametric space x^α; $\alpha \to -1$. The advantage of this dimensional regularization is that it does not interfere with algebraic rules; the regularized distributions satisfy the same relations as the singular ones, which is of great important for complex, analytical functions. For regularization of complex distributions one subtracts these poles as function of the order but with a fixed difference between the order of the singularity of p with respect to $\bar{p}$: $p^\alpha \bar{p}^{\alpha+k}$ with a fixed k [15].

We will follow a simpler approach with the same result. To avoid complications we define distributions of covariant objects only. Analyticity of the covariant object tells us the relation between p^+ and p^- at regularization. A homogeneous distribution is given by the partial integration of a singular, but integrable, function:

$$\left(\frac{1}{p^+}, \phi\right) = \int dp^- \frac{1}{p^+}\phi = \int dp^- \left[\frac{\partial}{\partial p^+}\ln(p^+p^-)\right]\phi. \tag{76}$$

We need p^+p^- for positive imaginary values. So we take the cut of the logarithm along the negative imaginary axis, therefore, the logarithm has an imaginary part of the form $i\pi\theta(-p^+p^-)$. The homogeneous distribution is

$$\frac{1}{[p^+]} \equiv \frac{\partial}{\partial p^+}[\ln|p^+p^-| + i\pi\theta(-p^+p^-)]$$
$$= \frac{1}{p^+ + i\epsilon\sigma(p^-)} = \mathrm{P}\frac{1}{p^+} - i\pi\sigma(p^-)\delta(p^+), \tag{77}$$

where P is the principal value. The result is that $\partial_{p^+}\partial_{p^-}\ln(p^+p^-) = \partial_{p^-}(p^+)^{-1} = 2\pi i\delta(p^-)\delta(p^+)$, which is nothing but the Mandelstam-Leibrandt regularization. (The i can be accounted for through Wick rotating the z variable.) After Fourier transformation the distribution $\ln(p^+p^- + i\epsilon)$ becomes a singular function which contains the intersection of the light cone with the null planes $x^+ = 0 \vee x^- = 0$: $\mathcal{F}[\ln(p^+p^- + i\epsilon)] = \frac{i\delta^2(x_\perp)}{x^+x^- - i\epsilon} = -\delta^2(x)\delta^1(x^+x^-) + i\delta^2(x_\perp)\mathrm{P}\frac{1}{x^+x^-}$. This fact is part of the reason why there exists confusion about the instantaneous term in the fermion propagator. In a Feynman diagram the integrands are treated as meromorphic functions in the complex plane. The real part is automatically complemented with a imaginary part. If we use a Hamiltonian approach we have constraints which relate real parts to real parts and we express one in terms of the other, therefore we might loose some information concerning the behavior of the imaginary parts. To put it in other words: the off-shell behavior comes naturally in a Feynman diagram and this does not always happen in a LCT-ordered diagram. This is another reason why we chose to define light-front field theory in close connection with a formulation in terms of Feynman diagrams.

VI. PROOF OF EQUIVALENCE

In this section we have collected several technical aspects of the proof of equivalence. In Sec. II we gave some examples, in order to illustrate the general procedure. Therefore, we do not give any examples here.

A. Energy integration

We present here the proof of the basic theorem on the integration over p^-. First we discuss the case of a single loop. The proof for several loops comes next.

1. One loop

The integration of a Feynman diagram over one energy loop variable p^- gives the following expression with the p^+-interval corresponding to $\{(\mathrm{Im}H_i > 0 \wedge i \leq m) \vee (\mathrm{Im}H_i < 0 \wedge i > m)\}$:

$$FD(\vec{H}) = \int \frac{dp^-}{2\pi} \frac{1}{2^N p_1^+ \cdots p_N^+ [p^- - H_1] \cdots [p^- - H_N]}$$
$$= \frac{i(-1)^{N+1}}{2^N (p_1^+ \cdots p_N^+) \Delta(H_1, \ldots, H_N)} \begin{vmatrix} H_1^{N-2} & \cdots & H_1^2 & H_1 & 0 & 1 \\ H_2^{N-2} & \cdots & H_2^2 & H_2 & 0 & 1 \\ \vdots & & & & \vdots & \vdots \\ H_m^{N-2} & \cdots & H_m^2 & H_m & 0 & 1 \\ H_{m+1}^{N-2} & \cdots & H_{m+1}^2 & H_{m+1} & 1 & 0 \\ \vdots & & & & \vdots & \vdots \\ H_N^{N-2} & \cdots & H_N^2 & H_N & 1 & 0 \end{vmatrix}. \quad (78)$$

The last factor is a complicated mixed symmetric polynomial in the H_i's that we denote by $(-1)^n W_{m,n}(H_1, \ldots, H_m | H_{m+1}, \ldots, H_{n+m})$. (The phase factor $(-1)^{N+1}$ is introduced to simplify the final expressions.) Δ is the Vandermonde determinant ($n \geq 2$):

$$\Delta(x_1 \cdots, x_n) = \det[\Delta_{ij}], \quad (79)$$
$$\Delta_{ij} = x_i^{n-j}. \quad (80)$$

A well known result is

$$\Delta(x_1 \cdots, x_n) = \prod_{i<j}^{n-1,n} (x_i - x_j). \quad (81)$$

See for instance MacDonald or Fulton and Harris [16] for properties of the Vandermonde determinant.

Proof. Depending on the (fixed) values of the (kinematical) p_i^+'s some poles are above and some are below the real axis. The integral is computed as $2\pi i$ times the sum of the residues. The residue of pole $p^- = H_i$ can be written as

$$(-1)^{i+1} \frac{\Delta(H_1, \ldots, H_{i-1}, H_{i+1}, \ldots, H_N)}{2^N (p_1^+ \cdots p_N^+) \Delta(H_1, \ldots, H_N)}. \quad (82)$$

We can add a line and a column to the determinant in the numerator:

$$(-1)^{i+1} \begin{vmatrix} H_1^{N-2} & \cdots & H_1^2 & H_1 & 1 \\ H_2^{N-2} & \cdots & H_2^2 & H_2 & 1 \\ \vdots & & & & \vdots \\ H_{i-1}^{N-2} & \cdots & H_{i-1}^2 & H_{i-1} & 1 \\ H_{i+1}^{N-2} & \cdots & H_{i+1}^2 & H_{i+1} & 1 \\ \vdots & & & & \vdots \\ H_N^{N-2} & \cdots & H_N^2 & H_N & 1 \end{vmatrix} = (-1)^{N+1} \begin{vmatrix} H_1^{N-2} & \cdots & H_1^2 & H_1 & 1 & 0 \\ H_2^{N-2} & \cdots & H_2^2 & H_2 & 1 & 0 \\ \vdots & & & & \vdots & \vdots \\ H_{i-1}^{N-2} & \cdots & H_{i-1}^2 & H_{i-1} & 1 & 0 \\ H_i^{N-2} & \cdots & H_i^2 & H_i & 1 & 1 \\ H_{i+1}^{N-2} & \cdots & H_{i+1}^2 & H_{i+1} & 1 & 0 \\ \vdots & & & & \vdots & \vdots \\ H_N^{N-2} & \cdots & H_N^2 & H_N & 1 & 0 \end{vmatrix}. \quad (83)$$

The final formula is obtained by adding determinants of type Eq. (83) which amounts to just adding their last columns. This gives the result stated in the theorem.

2. *Several loops*

In the case of several loops we integrate loop by loop. We must use the residue theorem such that the order of integration does not change the result. In general, the momenta of the particles on the internal lines will be linear combinations of the integration variables, say $k_i = \sum_k \alpha_i^k p_k$, where k_i^μ is the four-momentum on line i and p_k^μ is the integration variable. One has the freedom to choose the latter such that α_i^k is either $+1$, -1, or 0.

Theorem. Multi-dimensional energy integration. An unambiguous expression is

$$\int dp_1^- dp_2^- \cdots dp_m^- \prod_{i=1}^n \left(\sum \alpha_i^k p_k^- + H_i \right)^{-1} \quad (84)$$
$$= (2\pi i)^m \sum_{\substack{\{j_1, j_2, \ldots, j_m\} \\ [\alpha^1 \cdots \alpha^k]_{j_1 \cdots j_k} \neq 0}} \frac{1}{[\alpha^1 \alpha^2 \cdots \alpha^m]_{j_1 \cdots j_m}} \prod_{i \neq j_r}^n \left(\frac{[\alpha^1 \alpha^2 \cdots \alpha^m H]_{j_1 \cdots j_m i}}{[\alpha^1 \alpha^2 \cdots \alpha^m]_{j_1 \cdots j_m}} \right)^{-1}.$$

The antisymmetrized product $[\alpha^1 \cdots \alpha^m]_{j_1 \cdots j_m}$ is the determinant of the matrix

$$(\alpha)_{j_1 \cdots j_m} \equiv \alpha = \begin{pmatrix} \alpha^1_{j_1} & \cdots & \alpha^1_{j_m} \\ \vdots & & \vdots \\ \alpha^m_{j_1} & \cdots & \alpha^m_{j_m} \end{pmatrix}. \tag{85}$$

The inverse of the matrix α will be denoted by $\bar{\alpha}$. The poles $\{j_1, \cdots, j_m\}$ that are included in the sum have for all values of p_i^- the correct imaginary sign of H_j/α^i_j, because this sign is determined by the plus components of the integration variables. Before we start to integrate we first determine inside which contours the different poles lie, then drop the $i\epsilon$ description. This is clearly an invariant formulation, so the order of integration can be altered.

Proof. An unambiguous way to define the integration is to shift the integration contour slightly into the complex plane and leave the poles on the real axis. The poles are determined by the following set of linear equations:

$$\sum_i \alpha^i_k p_i^- + H_{j_k} = 0, \quad i,k = 1, \ldots, m, \tag{86}$$

which have the solution

$$\bar{p}_i^- = -\sum_k \bar{\alpha}^k_i H_k. \tag{87}$$

Next the multidimensional integral is written in terms of these new variables. The Jacobian of the transformation is $\det \bar{\alpha} = 1/\det \alpha = 1/[\alpha^1 \cdots \alpha^m]_{j_1 \cdots j_m}$. Subsequently, we apply the residue theorem to every $\bar{p}^-$ integration. We substitute the new variables, and find that the pole part of the integral factorizes:

$$\int \prod_{j=1}^n dz_j \frac{f(z)}{(\alpha^j_1 z_j - \gamma_1) \cdots (\alpha^j_m z_j - \gamma_m)}$$

$$= \det[\bar{\alpha}] \int dy_1 \frac{1}{y_1 - \bar{\alpha}^j_1 \gamma_j} \cdots \int dy_m \frac{1}{y_m - \bar{\alpha}^j_m \gamma_j} f(\bar{\alpha} y). \tag{88}$$

We used the summation convention. Note that the integral is independent of the choice of integration variables.

This type of multidimensional complex integration is not related to topology, so the deformation of the contour might change the result. The torus obtained by closing the different contours depends on the choice of coordinates. To avoid ambiguities we take an algebraic view instead.

B. Recursion formula

The recursion formula is the basis of the proof of equivalence. It tells us how to take out of any Feynman diagram the building block of a LCT-ordered diagram: an energy denominator. This happens without changing the structure of the algebraic form of the reduced Feynman diagram, so we can apply this formula a number of times (the recursion). The final result, obtained upon the last application of the recursion formula can immediately be evaluated. The final object is just a piece of a LCT-ordered diagram (TOD): a product of energy denominators.

The recursion formula allows us to consecutively pull energy denominators out of $FD(\vec{H})$ in order to obtain a sum of TOD's.

Theorem. The following identity is true for any m and n ($N = m + n$):

$$\frac{W_{m,n}(H_1, \ldots, H_m | H_{m+1}, \ldots, H_N)}{\Delta(H_1, \ldots, H_N)} = \frac{1}{H_1 - H_{m+1}} \left(\frac{W_{(m-1),n}(H_2, \ldots, H_m | H_{m+1}, \ldots, H_N)}{\Delta(H_2, \ldots, H_N)} \right.$$

$$\left. + \frac{W_{m,(n-1)}(H_1, \ldots, H_m | H_{m+2}, \ldots, H_N)}{\Delta(H_1, \ldots, H_m, H_{m+2}, \ldots, H_N)} \right). \tag{89}$$

Remark. The reduction step removes two poles, H_1 and H_{m+1}, and combines them into a single energy denominator, $H_1 - H_{m+1}$. The second factor of the RHS of Eq. (89) consists of two terms, both of which contain one pole less than the original form. The factor $(H_1 - H_{m+1})^{-1}$ is incorporated in the TOD. At the first stage, $W_{m,n}/\Delta$ is a structure that is directly related to a Feynman diagram. After taking steps in the reduction algorithm objects with the same structure are obtained, but these objects are not in the same way associated with (possibly different) Feynman diagrams. The last step in the algorithm is given by

$$W_{1,n}(y | x_1, \ldots, x_n) = W_{n,1}(x_1, \ldots, x_n | y) = \Delta(x_1, \ldots, x_n). \tag{90}$$

First we prove the formula (89) and then we show how to carry out the reduction.

Proof. First express $W_{m,n}$ in terms of a determinant as in Eq. (78). Then perform the usual manipulations with determinants: take linear combinations of rows or columns. If we subtract the first row from the rows 2 to m, the $m+1$st row from the other rows $\{m+2, \ldots, m+n\}$, and expand the determinant with respect to the last two columns, we obtain

$$W_{m,n}(x_1,\ldots,x_m|y_1,\ldots,y_n) = (-1)^N \begin{vmatrix} x_2^K - x_1^K & \cdots & x_2 - x_1 \\ \vdots & & \vdots \\ x_m^K - x_1^K & \cdots & x_m - x_1 \\ y_2^K - y_1^K & \cdots & y_2 - y_1 \\ \vdots & & \vdots \\ y_n^K - y_1^K & \cdots & y_n - y_1 \end{vmatrix}, \tag{91}$$

where $K = n + m - 2 = N - 2$. We can add a row and a column to the determinant to obtain

$$\frac{(-1)^{m+1}}{x_1 - y_1} \begin{vmatrix} x_2^K - x_1^K & \cdots & x_2 - x_1 & 0 \\ \vdots & & \vdots & \vdots \\ x_m^K - x_1^K & \cdots & x_m - x_1 & 0 \\ x_1^K - y_1^K & \cdots & x_1 - y_1 & x_1 - y_1 \\ y_2^K - y_1^K & \cdots & y_2 - y_1 & 0 \\ \vdots & & \vdots & \vdots \\ y_n^K - y_1^K & \cdots & y_n - y_1 & 0 \end{vmatrix}. \tag{92}$$

We split the determinant into two parts by adding and subtracting in the last column the column $(x_2 - x_1, \ldots, x_m - x_1, 0, \ldots, 0)$. Then we subtract the last column from the next to last column in both determinants to obtain

$$\frac{(-1)^{m+1}}{x_1 - y_1} \left(\begin{vmatrix} x_2^K - x_1^K & \cdots & 0 & x_2 - x_1 \\ \vdots & & \vdots & \vdots \\ x_m^K - x_1^K & \cdots & 0 & x_m - x_1 \\ x_1^K - y_1^K & \cdots & 0 & x_1 - y_1 \\ y_2^K - y_1^K & \cdots & y_2 - y_1 & 0 \\ \vdots & & \vdots & \vdots \\ y_n^K - y_1^K & \cdots & y_n - y_1 & 0 \end{vmatrix} - \begin{vmatrix} x_2^K - x_1^K & \cdots & 0 & x_2 - x_1 \\ \vdots & & \vdots & \vdots \\ x_m^K - x_1^K & \cdots & 0 & x_m - x_1 \\ x_1^K - y_1^K & \cdots & x_1 - y_1 & 0 \\ y_2^K - y_1^K & \cdots & y_2 - y_1 & 0 \\ \vdots & & \vdots & \vdots \\ y_n^K - y_1^K & \cdots & y_n - y_1 & 0 \end{vmatrix} \right). \tag{93}$$

We add the mth row to the rows above it in the first determinant, and subtract it from the rows below it in the second determinant. The result is

$$\frac{(-1)^{m+1}}{x_1 - y_1} \begin{vmatrix} x_2^K - y_1^K & \cdots & 0 & x_2 - y_1 \\ \vdots & & \vdots & \vdots \\ x_m^K - y_1^K & \cdots & 0 & x_m - y_1 \\ x_1^K - y_1^K & \cdots & 0 & x_1 - y_1 \\ y_2^K - y_1^K & \cdots & y_2 - y_1 & 0 \\ \vdots & & \vdots & \vdots \\ y_n^K - y_1^K & \cdots & y_n - y_1 & 0 \end{vmatrix} + \frac{(-1)^m}{x_1 - y_1} \begin{vmatrix} x_2^K - x_1^K & \cdots & 0 & x_2 - x_1 \\ \vdots & & \vdots & \vdots \\ x_m^K - x_1^K & \cdots & 0 & x_m - x_1 \\ x_1^K - y_1^K & \cdots & x_1 - y_1 & 0 \\ y_2^K - x_1^K & \cdots & y_2 - x_1 & 0 \\ \vdots & & \vdots & \vdots \\ y_n^K - x_1^K & \cdots & y_n - x_1 & 0 \end{vmatrix}. \tag{94}$$

Let $M = n + m - 3$ and define for any k the symmetric function ϕ by the relation $x^k - y^k = (x - y)\phi^{k-1}(x, y)$. The rows contain one of the factors $x_i - x_1$, $y_j - x_1$, $y_j - y_1$, or $x_i - x_1$, that can be divided out. The product of these factors are written as the ratio of two Vandermonde determinants, to obtain from Eq. (94)

$$\frac{(-1)^{m+1}}{x_1 - y_1} \left(\frac{\Delta(x_1 \cdots x_m, y_2 \cdots y_n, y_1)}{\Delta(x_1 \cdots x_m, y_2 \cdots y_n)} \begin{vmatrix} \phi^M(x_2, y_1) & \cdots & 0 & 1 \\ \vdots & & \vdots & \vdots \\ \phi^M(x_m, y_1) & \cdots & 0 & 1 \\ \phi^M(x_1, y_1) & \cdots & 0 & 1 \\ \phi^M(y_2, y_1) & \cdots & 1 & 0 \\ \vdots & & \vdots & \vdots \\ \phi^M(y_n, y_1) & \cdots & 1 & 0 \end{vmatrix} + \frac{\Delta(x_2 \cdots y_n, x_1)}{\Delta(x_2 \cdots y_n)} \begin{vmatrix} \phi^M(x_2, x_1) & \cdots & 0 & 1 \\ \vdots & & \vdots & \vdots \\ \phi^M(x_m, x_1) & \cdots & 0 & 1 \\ \phi^M(y_1, x_1) & \cdots & 1 & 0 \\ \phi^M(y_2, x_1) & \cdots & 1 & 0 \\ \vdots & & \vdots & \vdots \\ \phi^M(y_n, x_1) & \cdots & 1 & 0 \end{vmatrix} \right). \tag{95}$$

The dependence of the first determinant on y_1 is only apparent. The same is true for the dependence on x_1 of the second determinant. We can easily see this through matrix multiplication:

$$\begin{pmatrix} x_1^{n-2} & \cdots & x_1 & 1 & 1 \\ \vdots & & \vdots & \vdots & \vdots \\ x_m^{n-2} & \cdots & x_m & 1 & 1 \\ x_{m+1}^{n-2} & \cdots & x_{m+1} & 1 & 0 \\ \vdots & & \vdots & \vdots & \vdots \\ x_n^{n-2} & \cdots & x_n & 1 & 0 \end{pmatrix} \begin{pmatrix} 1 & 0 & \cdots & 0 & 0 \\ y & 1 & \ddots & \vdots & \vdots \\ \vdots & \ddots & \ddots & 0 & \vdots \\ y^{n-2} & \cdots & y & 1 & 0 \\ 0 & \cdots & 0 & 0 & 1 \end{pmatrix} = \begin{pmatrix} \phi^{n-2}(x_1,y) & \cdots & x_1+y & 1 & 1 \\ \vdots & & \vdots & \vdots & \vdots \\ \phi^{n-2}(x_m,y) & \cdots & x_m+y & 1 & 1 \\ \phi^{n-2}(x_{m+1},y) & \cdots & x_{m+1}+y & 1 & 0 \\ \vdots & & \vdots & \vdots & \vdots \\ \phi^{n-2}(x_n,y) & \cdots & x_n+y & 1 & 0 \end{pmatrix}. \tag{96}$$

The determinant of the second matrix at the LHS is 1, so the determinant of the first matrix at the LHS is the same as the determinant of the matrix at the RHS. Removing the y_1 dependence in the first determinant and the x_1 dependence in the second we get two familiar objects:

$$\frac{(-1)^n}{x_1-y_1}\left(\frac{-\Delta(x_1\cdots y_n)}{\Delta(x_1\cdots x_m,y_2\cdots y_n)} \begin{vmatrix} x_1^M & \cdots & x_1 & 0 & 1 \\ \vdots & & \vdots & \vdots & \vdots \\ x_m^M & \cdots & x_m & 0 & 1 \\ y_2^M & \cdots & y_2 & 1 & 0 \\ \vdots & & \vdots & \vdots & \vdots \\ y_n^M & \cdots & y_n & 1 & 0 \end{vmatrix} + \frac{\Delta(x_1\cdots y_n)}{\Delta(x_2\cdots y_n)} \begin{vmatrix} x_2^M & \cdots & x_2 & 0 & 1 \\ \vdots & & \vdots & \vdots & \vdots \\ x_m^M & \cdots & x_m & 0 & 1 \\ y_1^M & \cdots & y_1 & 1 & 0 \\ \vdots & & \vdots & \vdots & \vdots \\ y_n^M & \cdots & y_n & 1 & 0 \end{vmatrix} \right). \tag{97}$$

These determinants are nothing but W functions, but now with less arguments than we started with. So we can write Eq. (97) as

$$\frac{\Delta(x_1\cdots y_n)}{x_1-y_1}\left(\frac{W_{m,n-1}(x_1\cdots x_m|y_2\cdots y_n)}{\Delta(x_1\cdots x_m,y_2\cdots y_n)} + \frac{W_{m-1,n}(x_2\cdots x_m|y_1\cdots y_n)}{\Delta(x_2\cdots y_n)} \right). \tag{98}$$

If we divide the whole expression by $\Delta(x_1\cdots y_n)$ we get the reduction formula.

C. Reduction algorithm

We will now show that the application of the formula derived above gives us parts of LCT-ordered diagrams. First we need to specify the structure of a LCT-ordered diagram.

Definition. Loop connection tuple. The loop connection tuple $\vec{H}=\{H_1,\ldots,H_n\}$ is an ordered set of objects related to the propagator denominators $p_j^2-m_j^2+i\epsilon = 2p_j^+(p^- - H_j)$ or $H_j = p^- - p_j^- + \frac{p_{j\perp}^2+m_j^2}{2p_j^+}$. The ordering of the tuple corresponds to consecutive ordering of the internal lines in the corresponding loop in a Feynman diagram.

We will use the terminology of "lines" when we mean the corresponding momentum or energy, or state. There is some arbitrariness in the definition of the momenta in the loop, but in the objects of interest H_i-H_j this arbitrariness is gone because they are invariant under a shift of the loop momentum ($p^\mu \to p^\mu + a^\mu$). The expression H_i-H_j is the total incoming $\sum P_{\text{ext}}^-$ momentum minus the on-shell values of the minus momenta of the internal lines $p_{i,\text{on}}^- + p_{j,\text{on}}^-$, calculated with the help of $p_{i,j}^+$ and $p_{i,j}^\perp$. (See also Sec. II B.)

Definition. Backward and forward. A line i of the loop connection tuple is going backward if the object H_i has a positive imaginary part and is going forward if it has negative imaginary part. Thus in the Feynman diagram above, Eq. (78), $H_1,\ldots,H_m$ are going forward and $H_{m+1},\ldots,H_N$ are going backward. The sign of the imaginary part is opposite to the sign of the on-shell energy of the particle, therefore this definition of backward and forward coincides with the causality condition: positive-energy particles go forward in LC time and negative-energy particles go backward in LC time.

Definition. Early, late, and trivial events. An early event is a vertex between a backward and a forward going line, a late event is a vertex between a forward and a backward going line, if one goes around the loop in the order corresponding to the connection tuple. All other vertices are trivial events. There are equal numbers of early and late events.

Definition. Flat loop diagrams. A flat loop diagram has one early (and thus one late) event.

Definition. Crossed loop diagrams. A crossed loop has more than one early event.

Definition. Skeleton graph. A skeleton graph is the tuple of signs of the objects H_i of a connection tuple. It is given by the mapping $\{H_1,H_2,\ldots,H_n\} \to \{\sigma(\text{Im}H_1),\sigma(\text{Im}H_2),\ldots,\sigma(\text{Im}H_n)\}$. The function σ is the sign function.

For different external momenta in the Feynman graph we have a different set of skeleton graphs, and for each Feynman diagram there are a number of skeleton graphs. For each sector (associated with a specific number of poles above and below the real axis) of the loop momentum p^+ there is a skeleton graph, thus for a loop with n lines there are $n-1$ skeleton graphs.

The skeleton graph already tells us the general features of the LCT-ordered diagrams which are contained in a Feynman diagram, because it tells us the direction of the internal lines. This is used as our guide how to take "time slices" of the Feynman diagram. The direction of a line tells us in which order we can encounter events (vertices).

Early and late events correspond to sign changes in the skeleton graph.

Definition. Causally connected events. Two events are causally connected if they lie on the same loop and there are neither early nor late events lying in between.

So, two causally connected events are connected by parts of a loop that consist of lines that are either all forward or all backward.

Remark. Clearly, it makes sense to say that causally connected events are ordered in LC time. If we follow a loop in the direction given by the orientation defined by its connection tuple, then we will encounter forward and backward going lines. If two vertices are connected by a forward line, they are said to be ordered in LC time in the same way as they are ordered in the loop. Otherwise their order in LC time is the inverse of their order in the loop. This partial ordering, which is given by the skeleton graph, is obviously not complete. Only causally connected events are mutually ordered this way, but not with respect to other events.

Note that we don't make any statements here about reducible Feynman diagrams, which is a completely different story. Our causally unconnected parts connect up a later time, so they are parts of the same irreducible Feynman diagram.

Definition. Simultaneous. Two parts of a skeleton graph are said to be *simultaneous* if they do not share events that are causally connected.

Remark. The flat box that we discussed in Sec. II consisted of a late and an early vertex, connected by two distinct parts of the loop, one consisting of lines graded +, the other of lines graded −. The relative LCT-ordering of the events on these two parts is not necessarily determined by the skeleton graph, but application of the reduction formula, Eq. (89), produced immediately the two possible LCT orderings. The diagrams found showed the expected energy denominators.

In situations where two simultaneous parts occur, the reduction formula does not provide immediately the LCT-ordered diagrams. An example was given in Sec. II A 2. From the point of view of LC time ordering, one expects diagrams to occur corresponding to all relative LCT orderings of simultaneous parts. In momentum-energy language this means that diagrams with certain energy denominators should occur. Indeed, this is the content of the next theorem.

Theorem. Simultaneous parts come in all combinations.

Remark. The proof of this theorem relies again on a recursion. First we suppose that we have two simultaneous parts, that are already ordered by themselves, but not mutually. Both parts correspond to sets of energy denominators, say $\{\alpha\}$ and $\{\beta\}$. So we have the two distinct TOD's $\Pi\alpha_i^{-1}$ and $\Pi\beta_j^{-1}$. In this language the content of the theorem can be written as $\big\{\{i_k,j_k\}_k|[\{i_k,j_k\}\neq\{i_{k+1},j_{k+1}\}]\wedge[k<l\Rightarrow(i_k\leq i_l)\wedge(j_k\leq j_l)]\big\}$,

$$\prod_{i=1}^{m}\alpha_i^{-1}\prod_{j=1}^{n}\beta_j^{-1}=\sum_{\text{all } i_k,j_k}\prod_{k=1}^{m+n}(\alpha_{i_k}+\beta_{j_k})^{-1}. \tag{99}$$

Proof. We apply the formula

$$\prod_{i=1}^{m}\alpha_i^{-1}\prod_{j=1}^{n}\beta_j^{-1}=\frac{1}{\alpha_m+\beta_n}\left[\prod_{i=1}^{m-1}\alpha_i^{-1}\prod_{j=1}^{n}\beta_j^{-1}+\prod_{i=1}^{m}\alpha_i^{-1}\prod_{j=1}^{n-1}\beta_j^{-1}\right]. \tag{100}$$

We can apply this algorithm recursively to obtain $\binom{n+m}{m}$ TOD's with energy denominators of the form $\sum\alpha_i+\sum\beta_j$. If the product consists of more than two TOD's we can apply this algorithm recursively, to two TOD's at a time, since it is associative.

The expressions obtained are composite energy denominators:

$$[P^-(\alpha)-H_0(\alpha)]+[P^-(\beta)-H_0(\beta)]=P^-(\alpha\cup\beta)-H_0(\alpha\cup\beta). \tag{101}$$

D. Reduction of Feynman diagrams

The previous sections were mainly concerned with algebraic identities. Now we turn to the general strategy of the reduction. The reduction algorithm for a flat loop is straightforward as we noted when we discussed simultaneous parts. The trivial vertices come in all orderings of vertices on the forward line ($\mathrm{Im}H<0$) with respect to those on the backward line ($\mathrm{Im}H>0$). The vertices on one line are already ordered with respect to each other by the skeleton graph. Starting with the early event one can reduce the lines next to the early event. This algorithm ends and gives 2^{N-2} TOD's if the loop is flat for all skeleton graphs. For each skeleton graph there are $\binom{N-2}{m-1}$ TOD's.

Mapping. The mapping from a recursive algorithm to a time-ordered theory is straightforward for the flat loop. The order in which the poles H_i are removed in the reduction formula is the same as the time ordering. We refer to this reduction as time ordered reduction.

A flat Feynman diagram gives the topology of all TOD's contained in it and all combinations between trivial events appear respecting the causal order. Conservation of p^+ momentum determines whether a trivial vertex is an absorptive or emissive event. However, this is not a new element, because we have seen that a skeleton graph is determined by the external lines besides the value of the plus component of the loop momentum. Of course, early events absorb external particles while late events emit them.

Because Feynman diagrams form the basis of our treatment of light-front field theory, the basic elements we are concerned with are the single particle propagators and the vertices derived from the underlying Lagrangian. The interaction $\mathcal{H}_{\text{int}}$ is derived from $\mathcal{L}_{\text{int}}$ with an additional phase factor $(\sqrt{2^n p_1^+ p_2^+\cdots p_N^+})^{-1}$ where the longitudinal momenta of all the lines from a vertex are included. A wave function must also be multiplied with the phase factor, as compared to the covariant wave function.

For the success of our reduction algorithm the details of $\mathcal{L}_{\rm int}$ are of minor importance. The algebra is connected to plus-momentum flow in loops. The only internal lines in the diagram of interest are those in the loop; how momentum is extracted from and added to the loop is of less importance.

The most important feature of the reduction algorithm is the fact that it always starts from an early state with positive longitudinal momentum (there is always an early state as the result of momentum conservation), so we exclude "vacuum"-type diagrams.

First, reduction is performed on the skeleton graph starting from the early events, i.e., removing lines directly connected to the early events. This can be followed by removing poles corresponding to consecutive pieces of the loop until a late vertex is reached. This is the point where $W_{m,n}/\Delta$ is reduced to a sum of terms of the form $W_{j,1}/\Delta'$ or $W_{1,k}/\Delta''$. Secondly, the simultaneous-parts theorem is applied to write all these terms as sums of terms containing true energy denominators.

Because we could have started the reduction from the late vertices in stead of the early ones, we see that the algorithm can be written in different ways. The final result, however, is the same. The same is true, *mutatis mutandis*, for the application of the simultaneous-parts theorem.

So we peel off more and more of the Feynman diagram in a manner which is locally (for causally connected events) equal to time ordered reduction.

The relation of the results of the reduction process to LCT-ordered diagrams in the crossed loop case is more complicated than in the case of a flat loop. The simple heuristic of cutting lines representing constant LC time surfaces leads to a more elaborate bookkeeping in the crossed-loop case. This is so because only the global structure of the Feynman diagram determines which simultaneous parts are joined by early or late vertices. The general strategy proposed here is to start at an early vertex, use the reduction algorithm locally until a late vertex is attained. This procedure is to be repeated until all late vertices have been processed. Next apply the simultaneous-parts theorem repeatedly.

Extension mapping. Multiloop diagrams can be reduced one loop after another. The loop momenta that are not integrated over are kept fixed. The skeleton graph tells us again what is the general form of the time-ordered diagrams. Therefore, the skeleton graphs associated with different finite domains in p^+ space need to be determined first.

Upon application of the reduction algorithm to the first loop, energy denominators occur that are combinations of two propagator poles. When the next loop is treated, some poles come from those energy denominators, while the others are due to propagator poles occurring in the part of the original Feynman diagram unaltered by the reduction so far. These different types of poles play the same role in the integration of the next variable. The pole is again the difference of the p^- flow and the on-shell energies from the poles and their associated lines in the Feynman diagram. The question which lines must be combined to generate energy denominators is related to the imaginary parts of the propagator poles and thus answered when the skeleton graph is determined. During the reduction process these combinations remain fixed.

The integration is invariant under coordinate transformations and reordering of the integrations. The mapping from a recursive algorithm to a LCT-ordered approach is more complicated here than in the single-loop case, but in essence the same. The most complicated task is the construction of the skeleton graphs. After this job is done, the reduction algorithm is applied to one loop after another, and the interpretation of the result is the same as in the case of one loop.

Theorem. Spectrum condition. The spectrum condition $p^+ \geq 0$ holds for all particles in the internal loops of the Feynman diagram.

Proof. The spectrum condition follows from two ingredients. First, at any vertex there is conservation of four-momentum, in particular plus momentum. Secondly, lines with negative p^+, antiparticle lines, can be reinterpreted as particle lines with positive p^+ by reversing the direction of the four-momentum on such lines. This reversal is in agreement with four-momentum conservation and LCT ordering.

E. Algorithm proofs

In a number of cases we restricted ourselves to a recursive formula, which could be applied to any structure [17]. We gave a *rule* that could be applied successively and leads to LCT-ordered diagrams with the right structure. For the flat loop case we obtain all LCT-ordered diagrams, since the algorithm is unique, and directly related to a time-ordered picture. In the case of the crossed loop diagrams the algorithm is not unique; the rule could be applied to different parts of the structure at the same time. We could start with the reduction at one early vertex or another early vertex. Strictly speaking, this poses a problem only when the rule can be applied to overlapping regions of the structure; the different orders in which the rule is applied might lead to different answers. Our *conjecture* is that in our case the final answer is unique and does not depend on the order in which the rule is applied. We base this conjecture on the observation that each term obtained after applying the first rule (with the simultaneous parts still present) can be associated with a topological object, such that all terms give the complete set of objects with specific properties. The topology is invariant, thus unique and independent of the way it is obtained. We have checked this for a number of cases, and found it to hold in all these cases. Note that we used a similar argument for deriving an invariant multiloop integration.

We would rather have shown that the reduction algorithm would lead to all time-ordered diagrams which satisfy the spectrum condition, which would also be some kind of invariant, but this turned out to be too complicated a problem in the general case. Therefore we did not write down a general formula directly relating any Feynman diagram to the sum of LCT-ordered diagrams.

At the moment we satisfy at each step the spectrum

condition and allow all possible orderings. The global properties follows from the local ones.

VII. DISCUSSION

We have established the degree of equivalence between light-cone-time ordered perturbation theory and covariant perturbation theory for spin-0 and spin-$\frac{1}{2}$ particles. This effort might seem superfluous since the connection between ordinary time-ordered perturbation theory and covariant perturbation theory is well established [18]. One might be tempted to believe that the methods that work in the case of ordinary time-dependent perturbation theory apply to the LCT-ordered theory too. This belief belongs to folklore. In practice the understanding of light-front field theory is growing only slowly. Basic results in covariant field theory were often proven to obtain also in light-front field theory along a path through much trial and error. It took years to obtain a proper light-front version of the Schwinger model [19] and to prove spontaneous symmetry breaking in the light-front version of ϕ^4 [20]. The renormalization of light-front versions of known covariant, renormalizable field theories is still an unsolved problem [21]. In general, approaches are followed that are specially tuned to the problems of light-front field theory. Therefore it turns out to be difficult to relate the solutions obtained to basic results in covariant field theory [22,23].

Conceptual problems were already present from the onset of light-front field theory, when Weinberg showed [6] that only some physical processes, each represented by an ordinary time-ordered diagram, contribute to the Feynman diagram if this diagram was calculated in a frame that moves with the speed of light [24]. This so called *infinite momentum frame* (IMF) cannot be connected to any other reference reference frame by a finite Lorentz transformation. Thus a limiting procedure is involved. This limit has to compete with other limits present in field theory: infinite space integration, regularization of singular expressions. This is separate from the additional problems that might arise when we are dealing with fermions [25]. That the IMF is naturally described with light-front coordinates is only apparent for coordinates and momenta [26]. That only some diagrams survive [7] is puzzling. However, we have shown that this, in general, is indeed true. Another possible approach to light-front field theory is the direct quantization on a light front. There are many different ways to do this, which become more elaborate if the theories are supposed to incorporate more features [27]. As a classical theory, light-front field theory is ill defined; the standard initial values problem on the light front is overdetermined. In addition, it leads to a nonunique evolution in time [8]. The first problem can be solved in principle through methods devised for the quantization of constrained systems [28]. The second problem is more serious. One needs to introduce degrees of freedoms associated with different evolutions in LC time and then introduce constraints which can restrict the space of solutions to the one considered physical on some grounds. This, in essence, is what people are dealing with when they introduce zero modes, degrees of freedom of which the evolution is unknown (zero or infinite?). This problem is often disguised in practical calculations where a $(p^+)^{-1}$ singularity occurs [29,30].

Another way to quantize a light-front theory is to use axiomatic commutation relations on a complete set of free fields [31–33], an approach guided by the results of current algebra [5]. On the light front, different points with $(\Delta x_\perp = 0)$ are lightlike separated. The question arises as to what is the equal-time commutator between fields: a δ function in x^- which violates covariance, or a sign function in x^- which leads to nonintegrable fields (except at the loss of covariance) [11]? Whether such theories can describe physical processes has not been established. This approach became less favorable in the late seventies. The approach most favored nowadays is based on two methods: with the covariant results in mind derive a "constrained Hamiltonian" [12,34,35]. Because of to zero modes it is hard to make a one-to-one correspondence between normalized states on a spacelike surface and a lightlike surface. As long as one deals only with tree graphs all these problems are rather formal. The presence of loops makes them acute. In loops one has to "sum over all states." This rule forces one to think over states with $p^+ \to 0$. The advantages of light-front field theory are paid for by the occurrence of problems. In the approaches discussed here the problems arise in different forms and are dealt with in different ways. They might be disguised as technical difficulties. Because of the fundamental nature of these problems the final results depend strongly on the choices one has to make when defining the (finite) theory, e.g., boundary conditions of fields quantized in a box [36,37], or regularization of the $(p^+)^{-1}$ singularity [29]. We also had to make some choices. Wherever we had to do so, we emphasized the relation with Feynman diagrams. In a manifestly covariant approach there is no $(p^+)^{-1}$ singularity. It is a distinct advantage of our approach that this singularity also does not occur (see Sec. V). We seem to have cured one of the diseases of light-front field theory. However, presently we do not know whether our regularization procedure leads to the same answer as the covariant approach.

We have shown (see Sec. V A) that in some cases there are $\delta(p^+)$ contributions to the S matrix. Maybe these terms indicate a coupling to the "vacuum" or they may represent contributions which relate one version of light-front field theory to another by a finite renormalization. However, it would be good practice to try to separate the mathematical question (how to calculate?) from the physical one (how to interpret?).

We consider the present situation in light-front field theory to be confused. We give three reasons for this point of view (i) the paucity of comparisons to standard covariant theories; (ii) the mixing of mathematical problems with physical ones; (iii) the lack of consensus on what are the established results (with proper, mathematically rigorous derivations). Still, there are a four good reasons to work on light-front field theory.

(a) It is the only theory distinctly different from covariant field theory which allows for a comparison at in-

termediate levels. Such a comparison increases the understanding in both theories.

(b) It is the most natural way to describe nucleons in terms of quarks.

(c) Our understanding increases with each answer to questions that light-front field theory raises.

(d) It is a Hamiltonian formulation, sharing the intuitive picture inherent in elementary quantum mechanics.

ACKNOWLEDGMENTS

The work described in this paper is part of the research program of the "Stichting voor Fundamenteel Onderzoek der Materie (FOM)," which is financially supported by the "Nederlandse Organisatie voor Wetenschappelijk Onderzoek (NWO)."

[1] P.A.M. Dirac, Rev. Mod. Phys. **21**, 392 (1949).
[2] J. Schwinger, *Selected Papers on Quantum Electrodynamics* (Dover, New York, 1958).
[3] H. Leutwyler and J. Stern, Ann. Phys. (N.Y.) **112**, 94 (1978).
[4] F.M. Lev, Riv. Nuovo Cimento **16**, 1 (1993).
[5] V. de Alfaro, S. Fubini, G. Furlan, and C. Rossetti, *Currents in Hadron Physics* (North-Holland, Amsterdam, 1973).
[6] S. Weinberg, Phys. Rev. **150**, 1313 (1966).
[7] S.-J. Chang and S.-K. Ma, Phys. Rev. **180**, 1506 (1969).
[8] L. Hörmander, *Linear Partial Differential Operators* (Springer-Verlag, Berlin, 1963), Sec. 5.2.
[9] S.-J. Chang, R.G. Root, and T.-M. Yan, Phys. Rev. D **7**, 1173 (1973).
[10] D.G. Robertson and G. McCartor, Z. Phys. C **53**, 661 (1992); S.J. Brodsky and A. Langnau, J. Comput. Phys. **109**, 84 (1993); a different approach related to cutting rules is pursued by Karmanov: V.G. Kadeshevsky, Zh. Eksp. Teor. Fiz. **46**, 654 (1964); **46**, 872, (1964) [Sov. Phys. JETP **19**, 443 (1964); **19**, 597 (1964)]; V.A. Karmanov, Fiz. Elem. Chastits At. Yadra **19**, 525 (1988) [Sov. J. Part. Nucl. **19**, 228 (1988)]; V.A. Karmanov (private communication).
[11] N. Nakanishi and K. Yamawaki, Nucl. Phys. **B122**, 15 (1977).
[12] J.B. Kogut and D.E. Soper, Phys. Rev. D **1**, 2901 (1970).
[13] S.-J. Chang and T.-H. Yan, Phys. Rev. D **7**, 1147 (1973).
[14] T.-H. Yan, Phys. Rev. D **7**, 1780 (1973).
[15] I.M. Gel'fand and G. Shilov, *Generalized Functions* (Academic Press, New York, 1964), Vol. 1, Appendix B.
[16] I.G. MacDonald, *Symmetric Functions and Hall Polynomials* (Clarendon Press, Oxford, 1979); W. Fulton and J. Harris, *Representation Theory* (Springer, New York, 1991).
[17] J.A. Bergstra and J.W. Klop, *Termherschrijfsystemen* (Kluwer Bedrijfswetenschappen, Deventer, The Netherlands, 1989).
[18] R.P. Feynman, Phys. Rev. **76**, 769 (1949).
[19] G. McCartor, Z. Phys. C **41**, 271 (1988); T. Heinzl, S. Krusche, and E. Werner, Phys. Lett. B **256**, 55 (1991).
[20] S.S. Pinsky and B. van de Sande, Phys. Rev. D **49**, 2001 (1994); T. Heinzl, S. Krusche, S. Simburger, and E. Werner, Z. Phys. C **56**, 415 (1992); T. Heinzl, S. Krusche, S. Simburger, and E. Werner, Phys. Lett. B **272**, 54 (1991); D.G. Robertson, Phys. Rev. D **47**, 2549 (1993).
[21] R.J. Perry, Phys. Lett. B **300**, 8 (1993); R.J. Perry, Ann. Phys. (N.Y.) **232**, 116 (1994); R.J. Perry and K.G. Wilson, Nucl. Phys. **B403**, 587 (1993); St.D. Głazek and K. G. Wilson, Phys. Rev. D **48**, 5863 (1993).
[22] C.B. Thorn, Phys. Rev. D **20**, 1934 (1979).
[23] D. Mustaki, S. Pinsky, J. Shigemitsu, and K. Wilson, Phys. Rev. D **43**, 3411 (1991).
[24] J. Kogut and L. Susskind, Phys. Rep. **8**, 75 (1973).
[25] D.V. Ahluwalia, Phys. Lett. B **277**, 243 (1992).
[26] H. Leutwyler, J.R. Klauder, and L. Streit, Nuovo Cimento **LXVIA**, 536 (1970).
[27] A.C. Kalloniatis and D.G. Robertson, Phys. Rev. D **50**, 5262 (1994).
[28] P.A.M. Dirac, *Lectures on Quantum Mechanics* (Yeshiva University Press, New York, 1964); A.J. Hanson, T. Regge, and C. Teitelboim, *Constrained Hamiltonian Systems* (Accademia Nazionale dei Lincei, Roma, 1976); M. Henneaux and C. Teitelboim, *Quantization of Gauge Systems* (Princeton University Press, Princeton, 1993); K. Sundermeyer, *Constrained Dynamics*, Lecture Notes in Physics Vol. 169 (Springer-Verlag, Berlin, 1982); L. Faddeev and R. Jackiw, Phys. Rev. Lett. **60**, 1692 (1988).
[29] M. Burkhardt, Phys. Rev. D **47**, 4628 (1993); P. Griffin, *ibid.* **46**, 3538 (1992); T. Maskawa and K. Yamazaki, Prog. Theor. Phys. **56**, 270 (1976); A.C. Tang, Phys. Rev. D **37**, 3014 (1988).
[30] M. Burkhardt and A. Langnau, Phys. Rev. D **44**, 3857 (1991).
[31] R. Jackiw, in *Canonical Light-Cone Commutators and Their Application*, Springer Tracts in Modern Physics Vol. 62, edited by G. Höhler (Springer-Verlag, Berlin, 1972).
[32] M. Ida, Nuovo Cimento A **40**, 354 (1977).
[33] S. Schlieder and E. Seiler, Commun. Math. Phys. **25**, 62 (1972).
[34] S.J. Brodsky, R. Roskies, and R. Suaya, Phys. Rev. D **8**, 4574 (1973).
[35] D. Mustaki, Phys. Rev. D **42**, 1184 (1990).
[36] R. A. Neville and F. Rohrlich, Nuovo Cimento **1A**, 625 (1971).
[37] S. Huang and W. Lin, Ann. Phys. (N.Y.) **226**, 248 (1993).